Title

T-cell Dysfunction upon Expression of MYC with Altered Phosphorylation at Threonine 58 and Serine 62.

Journal

Molecular Cancer Research, 20(7)

Authors

Daniel, Colin
Pelz, Carl
Wang, Xiaoyan
et al.

Publication Date

2022-07-06

DOI

10.1158/1541-7786.MCR-21-0560

Peer reviewed

T-cell Dysfunction upon Expression of MYC with Altered Phosphorylation at Threonine 58 and Serine 62

Colin J. Daniel[1], Carl Pelz[1], Xiaoyan Wang[1], Michael W. Munks[2], Aaron Ko[2], Dhaarini Murugan[3], Sarah A. Byers[1], Eleonora Juarez[1], Karyn L. Taylor[1], Guang Fan[4], Lisa M. Coussens[3,5], Jason M. Link[1], and Rosalie C. Sears[1,5]

ABSTRACT

As a transcription factor that promotes cell growth, proliferation, and apoptosis, c-MYC (MYC) expression in the cell is tightly controlled. Disruption of oncogenic signaling pathways in human cancers can increase MYC protein stability, due to altered phosphorylation ratios at two highly conserved sites, Threonine 58 (T58) and Serine 62 (S62). The T58 to Alanine mutant (T58A) of MYC mimics the stabilized, S62 phosphorylated, and highly oncogenic form of MYC. The S62A mutant is also stabilized, lacks phosphorylation at both Serine 62 and Threonine 58, and has been shown to be nontransforming *in vitro*. However, several regulatory proteins are reported to associate with MYC lacking phosphorylation at S62 and T58, and the role this form of MYC plays in MYC transcriptional output and *in vivo* oncogenic function is understudied. We generated conditional *c-Myc* knock-in mice in which the expression of wild-type MYC (MYC^{WT}), the T58A mutant (MYC^{T58A}), or the S62A mutant (MYC^{S62A}) with or without expression of endogenous *Myc* is controlled by the T-cell–specific *Lck*-Cre recombinase. MYC^{T58A} expressing mice developed clonal T-cell lymphomas with 100% penetrance and conditional knock-out of endogenous *Myc* accelerated this lymphomagenesis. In contrast, MYC^{S62A} mice developed clonal T-cell lymphomas at a much lower penetrance, and the loss of endogenous MYC reduced the penetrance while increasing the appearance of a non-transgene driven B-cell lymphoma with splenomegaly. Together, our study highlights the importance of regulated phosphorylation of MYC at T58 and S62 for T-cell transformation.

Implications: Dysregulation of phosphorylation at conserved T58 and S62 residues of MYC differentially affects T-cell development and lymphomagenesis.

Introduction

The c-MYC oncoprotein (MYC) plays an important role as a transcription factor in balancing cellular growth, proliferation, differentiation, and programmed cell death through the regulation of many target genes. The ability to promote cell growth and proliferation is modulated by MYC's ability to also promote apoptosis, which feasibly occurs in normal cells as a part of a feedback loop in response to high levels of MYC to keep proliferation in balance. With such important biological functions, it is not surprising that *Myc* knock-out mice are embryonically lethal and MYC null cells have severe growth and proliferation defects, while sustained overexpression of MYC in mice leads to cancer (1–3). Increased levels of MYC protein have been reported in about 70% of human cancers, but only approximately 20% of these show *MYC* gene amplification suggesting a role of posttranslational deregulation (4, 5). Studies have also shown that mutations in *MYC*, primarily at or around the conserved Threonine 58 (T58) and Serine 62 (S62) phosphorylation sites, are found in viral isolates, B-cell Burkitt lymphomas, and AIDS associated B- and T-cell lymphomas (6–9). Together, these observations support the importance of posttranslational regulation of MYC.

Normal cycling cells regulate the levels of MYC by tightly controlling its transcription, translation, and protein stability. One mechanism regulating MYC protein stability includes the sequential phosphorylation of two highly conserved phosphorylation sites at residues T58 and S62 in the transactivation domain (TAD) region (10–12). In response to growth signals, MYC is phosphorylated at S62 by one of several proline-directed kinases including ERK or CDKs, which transiently increases MYC stability. Subsequently, the phosphorylation at T58 is mediated by the processive kinase GSK3β (10) or BRD4 (13), initiating the dephosphorylation of S62 by Protein Phosphatase 2A (PP2A) and the ubiquitination of MYC by the E3 ligase complex SCF-FBW7, directing proteasomal degradation. The dephosphorylation at S62 is facilitated by the peptidyl prolyl isomerase, PIN1, which catalyzes a *cis* to *trans* isomerization at proline 63 (11, 14). This tightly regulated MYC degradation pathway is coordinated by the scaffold protein AXIN1 (15, 16), which is a known tumor suppressor (17, 18). The genes involved in this MYC degradation pathway such as *FBW7*, *AXIN1*, and the *PP2A* subunits, as well as proteins upregulating ERK and CDK kinase activity have been reported mutated in cancer cells including hematologic cancers and play a role in the widespread deregulated MYC phosphorylation and increased protein stability in tumors (15, 16, 19–23).

In addition to controlling MYC protein degradation, functional studies with the MYC T58A and S62A mutants have reported altered MYC activity indicating that aberrant phosphorylation at these sites

[1]Department of Molecular and Medical Genetics, School of Medicine, Oregon Health and Science University, Portland, Oregon. [2]Department of Molecular Microbiology and Immunology, School of Medicine, Oregon Health and Science University, Portland, Oregon. [3]Department of Cell, Developmental and Cancer Biology, School of Medicine, Oregon Health and Science University, Portland, Oregon. [4]Department of Pathology, School of Medicine, Oregon Health and Science University, Portland, Oregon. [5]Knight Cancer Institute, Oregon Health and Science University, Portland, Oregon.

Note: Supplementary data for this article are available at Molecular Cancer Research Online (http://mcr.aacrjournals.org/).

Corresponding Author: Rosalie C. Sears, Department of Molecular and Medical Genetics, Oregon Health and Sciences University, 2730 SW Moody Avenue, Portland, OR 97201. Phone: 503-494-6885; Fax: 503-494-4411; E-mail: searsr@ohsu.edu

Mol Cancer Res 2022;20:1151–65

doi: 10.1158/1541-7786.MCR-21-0560

can impact MYC function. The T58A mutation leads to increased levels of S62 phosphorylation and increased protein stability whereas the S62A mutant cannot be phosphorylated at either residue, which also generally leads to increased stability as it cannot be regulated through the S62/T58-mediated degradation pathway (11). Functionally, *in vitro* studies with fibroblasts and epithelial cells indicate that the T58A mutant (MYC^{T58A}) has increased transforming and DNA binding activity and the S62A mutant (MYC^{S62A}) has decreased transforming and DNA binding activity relative to wild-type MYC ((MYC^{WT}; refs. 24–27). This increased oncogenic potential of MYC^{T58A} may be in part due to a decreased capacity of MYC^{T58A} to induce apoptosis, which has been shown in tissue culture and mouse models (27–30). Consistently, human tumors and cancer cell lines display an altered ratio of decreased T58 to increased S62 phosphorylation, which correlates with impairment in the degradation pathway and increased MYC protein stability, has been broadly observed (16, 20, 29).

Mutations in *c-MYC* are rare and only appreciably observed in Burkitt and AIDS-associated lymphomas. These mutations occur at hot spots around the T58 and S62 residues, with previous studies reporting the predominant mutations to be T58I and T58A (7, 24, 31). Phospho-peptide mapping analysis of the T58I mutant has shown that unlike the T58A mutant, which has higher than wildtype S62 phosphorylation, MYC^{T58I} lacks phosphorylation at both the T58 and S62 sites suggesting that MYC lacking S62 phosphorylation can be oncogenic in B-cell lymphomagenesis (24). Thus, studying the effects of phosphorylation mutants at both T58 and S62 on MYC function and involvement in tumorigenesis *in vivo* remains an important area of research (6, 7), particularly for the MYC^{S62A} mutant which is not phosphorylated at either residue, shows low oncogenic activity *in vitro*, and has been understudied *in vivo*. This mutant has been previously observed using a mammary expressing Cre recombinase (Cre) with leaky expression in the brain to drive choroid plexus and pituitary tumors in mouse brain (29), however further examination of MYC^{S62A} *in vivo* function is lacking.

High levels of MYC have been broadly observed in human T-ALLs, due to a variety of mechanisms including a rare *MYC* gene translocation (32), frequent aberrant NOTCH1 signaling, and FBW7 mutations (19, 33–35), which are associated with increased MYC protein stabilization (33, 36–38). Given these observations of increased MYC stabilization in T-ALL (19, 20), in this study, we investigated the oncogenic potential of the two phosphorylation mutants of MYC utilizing our conditional knock-in mouse model expressing Myc^{WT}, Myc^{T58A}, or Myc^{S62A} from the endogenous *ROSA26* locus in response to Cre-mediated excision of a transcription stop site and the T-cell–specific *Lck*-Cre to mediate recombination (29, 30, 39–41). This model allows for the study of the MYC phosphorylation mutants in cells that pass through distinct phases of growth, proliferation, and apoptosis, allowing elucidation of the function of MYC without phosphorylation at T58 and/or S62 in T-cell development and lymphomagenesis.

Materials and Methods

Generation of *ROSA26*-floxed stop–c-Myc^{WT}, *ROSA26*-floxed stop–c-Myc^{T58A}, and *ROSA26*-floxed stop–c-Myc^{S62A} mice

ROSA26-floxed stop (RFS)--*c-Myc*^{WT}, *-c-Myc*^{T58A}, and *-c-Myc* ^{S62A} mice have been previously described (29). RFS-*c-Myc*^{WT}, *-c-Myc*^{T58A}, and *-c-Myc* ^{S62A} mice were crossed with *Lck*-Cre mice for T-cell–specific expression (30). To conditionally ablate endogenous *Myc*, RFS-$Myc^{WT}Myc^{fl/fl}$ *Lck*-Cre, RFS-$Myc^{T58A}Myc^{fl/fl}$ *Lck*-Cre, and RFS-$Myc^{S62A}Myc^{fl/fl}$ *Lck*-Cre mice ($MYC^{WT}MYC^{fl/fl}$, $MYC^{T58A}MYC^{fl/fl}$, & $MYC^{S62A}MYC^{fl/fl}$) were generated by breeding with C57Bl/6 conditional $Myc^{fl/fl}$ mice (42, 43). Simultaneously, cohorts of RFS-*c-Myc*^{WT}, *-c-Myc*^{T58A}, and *-c-Myc* ^{S62A} mice were generated by breeding out the $Myc^{fl/fl}$ allele to control for strain background in lymphomagenesis. Male or female control mice were homozygous for either RFS-Myc^{WT}, RFS-$Myc^{WT}Myc^{fl/fl}$, RFS-Myc^{T58A}, RFS-$Myc^{T58A}Myc^{fl/fl}$, RFS-Myc^{S62A}, RFS-$Myc^{S62A}Myc^{fl/fl}$ or $Myc^{fl/fl}$ mice, but had no *Lck*-Cre allele. All mice were handled and maintained in accordance with the Oregon Health and Science University (OHSU; Portland, OR) Institutional Animal Care and Use Committee.

Detection of recombination and genotyping

Lck-Cre mediated recombination in RFS-*c-Myc*^{WT}, *-c-Myc*^{T58A}, and *-c-Myc* ^{S62A} mice were determined by PCR analysis and specific primer sets. Genotyping for the presence of RFS, $Myc^{fl/fl}$ and *Lck*-Cre was done using tail DNA and specific primer sets (see Supplementary Table S1 for primer sequences).

Tumorigenesis surveillance

All cohorts of male or female experimental mice and control mice with no Cre expression were monitored for development of thymic lymphoma, splenomegaly, or both. Mice were subjected to euthanasia and necropsied when presented with accelerated breathing, a distended abdomen, cachexia, were moribund, and/or reached about 730 days of age. Kaplan–Meier survival plot was done using Prism (Graphpad Software Inc., RRID:SCR_002798).

qRT-PCR analysis

RNA was extracted from male and female mice with thymic lymphomas or normal thymi from control mice of any genotype with no Cre expression with Trizol (Invitrogen) following the manufacturer's protocol. The resulting RNA was treated with DNaseI (Roche) and further purified with a RNeasy mini kit (Qiagen). cDNA was synthesized using random primers with the High Capacity Reverse Transcription kit (Applied Biosystems). qRT-PCR for total, ectopic, and endogenous *c-Myc* mRNA was carried out on a StepOne qRT-PCR machine (Applied Biosystems) with SYBR Green (Invitrogen) and normalized to *Tbp* message (see Supplementary Table S2 for primer sequences).

T-cell survival and proliferation

Thymi and spleens were harvested from male or female 6-week–old experimental mice. Littermate controls were male or female mice homozygous for either RFS-Myc^{WT}, RFS-Myc^{T58A}, RFS-$Myc^{T58A}Myc^{fl/fl}$, RFS-Myc^{S62A}, or RFS-$Myc^{S62A}Myc^{fl/fl}$ with no Cre expression. Tissue was disrupted into a single cell suspension in 1X PBS with 5% FBS, 0.5% BSA, and 2 mmol/L EDTA and filtered through a 70-μm mesh filter. Cells were spun down at 1,200 rpm for 5 minutes. Red blood cells were lysed using RBC lysis buffer (155 mmol/L NH_4Cl, 12 mmol/L $NaHCO_3$, 0.1 mmol/L EDTA) Cells were respun and refiltered through a 70-μm mesh filter and counted. Two million splenocytes were plated per well (DMEM with 10% FBS, 4.5 g/L glucose, 2 mmol/L L-glut, NEAA, and 50 μmol/L β-mercaptoethanol) labeled with BrdU and stimulated with 1 μg Concanavalin A (Con A; Sigma-Aldrich) for 24 hours. FITC or APC BrdU Flow Kit (BD Pharmigen) and antibodies for CD4 (GK1.5, Thermo Fisher Scientific, catalog no. 553051, RRID:AB_464902) and CD8 (53–6.7, Thermo Fisher Scientific, catalog no. 553033, RRID:AB_467086) were used to assess CD4 and CD8 labeled splenic T-cell proliferation. Apoptosis of CD4- and CD8-positive ($CD4^+$, $CD8^+$) thymic T cells were assayed using a FITC Annexin V Apoptosis Detection Kit (BD Pharmigen)

24 hours postculture. Cells were analyzed with a BD FACS Canto II (BD Biosciences) and 100,000 live cell events were collected. Data files were analyzed using FlowJo X (Tree Star, Inc., RRID:SCR_008520).

Hematoxylin and eosin and immunofluorescence staining

Tissues were fixed in 10% formalin overnight at 4°C, washed in 70% EtOH the following day, and embedded in paraffin. A microtome (Leica) was used to cut 5-μm–thick sections, which were stained with Mayer hematoxylin and eosin (H&E). For immunofluorescence (IF) staining, antigen retrieval was achieved by pressure-cooking in citrate buffer pH 6 for 10 minutes (Sigma-Aldrich). Slides were allowed to cool for 1 hour. The following antibodies were used for staining: CD3 1:50 (pAb, Dako, catalog no. A045229–2, RRID:AB_2335677), CD45R 1:50 (RA3–6B2, Abcam, catalog no. ab64100, RRID:AB_1140036), pS62 MYC rat monoclonal (4B12, conjugated to AF647) 1:25 (44). Secondary antibodies include Alexa Fluor 488 and Alexa Fluor 750 (Invitrogen) and mounting media with antifade containing DAPI (Thermo Fisher Scientific). H&E and IF stains were imaged using a Zeiss Axio Scan.Z1 slide scanner at 20x and 40x. Analysis was done with Zen software (Zeiss Microscopy) and FIJI (RRID:SCR_002285).

Immunophenotyping

Tumor and control thymic tissue were disrupted into a single-cell suspension in 1X PBS with 5% FBS, 0.5% BSA, and 2 mmol/L EDTA and filtered through a 70-μm mesh filter. Cells were spun down at 1,200 rpm for 5 minutes, resuspended in 70% DMEM, 10% DMSO, 20% FBS, and frozen and stored at −80°C. Cells were stained in 1X PBS with 2% FBS and 0.1% NaN_3 for 20 minutes, on ice in the dark. Antibodies used are as follows: CD4-BUV737 (GK1.5, BD Biosciences, catalog no. 612761, RRID:AB_2870092), CD8-BUV395 (53–6.7, BD Biosciences, catalog no. 563786, RRID:AB_2732919), CD24-PE (M1/69, BD Biosciences, catalog no. 553262, RRID:AB_394741), CD25-BV650 (PC61, BD Biosciences, catalog no. 564021, RRID:AB_2738547), CD45-BUV496 (30F-11, BD Biosciences, catalog no. 749889, RRID:AB_2874129), CD138-PE (281–2, BD Biosciences, catalog no. 553714, RRID:AB_395000), Ly6G-BUV395 (1A8, BD Biosciences, catalog no. 565964, RRID:AB_2739417), and TCRβ-BUV737 (H57–597, BD Biosciences, catalog no. 612821, RRID:AB_2870145), CD4-PE/Cy7 (RM4–5, BioLegend, catalog no. 100528, RRID:AB_312729), CD8-PE/Cy7 (53–6.7, BioLegend, catalog no. 100722, RRID:AB_312761), CD19-BV650 (6D5, BioLegend, catalog no. 115541, RRID:AB_11204087), CD19-PerCP/Cy5.5 (6D5, BioLegend, catalog no. 115534, RRID:AB_2072925), CD21-APC/Cy7 (7E9, BioLegend, catalog no. 123417, RRID:AB_1953274), CD44-FITC (IM7, BioLegend, catalog no. 103021, RRID:AB_493684), CD49β-APC/Cy7 (DX5, BioLegend, catalog no. 108920, RRID:AB_2561458), B220-BUV395 (RA3–6B2, BD Biosciences, catalog no. 563793, RRID:AB_2738427), IgD-A488 (11–26c.2a, BioLegend, catalog no. 405718, RRID:AB_10730619), Sca-I-BV711 (D7, BioLegend, catalog no. 108131, RRID:AB_2562241), MHC II-BV421 (M5/114, BioLegend, catalog no. 107631, RRID:AB_10900075), Thy1.2-BV785 (30-H12, BioLegend, catalog no. 105331, RRID:AB_2562900), DAPI (BioLegend, catalog no. 422801), CD11b-FITC (M1/70, Thermo Fisher Scientific, catalog no. 11–0112–82, RRID:AB_464935), CD11c-PE (N418, Thermo Fisher Scientific, catalog no. 12–0114–81, RRID:AB_465551), CD23-PE/Cy7 (B3B4, Thermo Fisher Scientific, catalog no. 25–0232–82, RRID:AB_469604), B220-A647 (RA3–6B2, BioLegend, catalog no. 103226, RRID:AB_389330), Ly-6C-PerCP/Cy5.5 (HK1.4, Thermo Fisher Scientific, catalog no. 45–5932–82, RRID:AB_2723343), TACI-APC (ebio8F10–3, Thermo Fisher Scientific, catalog no. 17–5942–81, RRID:AB_842759), and TCRγδ-A647 (eBioGL3, Thermo Fisher Scientific, catalog no. 17–5711–82, RRID:AB_842756), IgM-BV421 (pAb, Jackson ImmunoResearch Labs, catalog no. 115–675–075, RRID:AB_2651085). Cells were analyzed with a BD FACS Symphony A5 (BD Biosciences). Data files were analyzed using FlowJo X (Tree Star, Inc., RRID:SCR_008520).

Generation of tumor cell lines

Tumor cell lines were generated as previously described in Jinadasa and colleagues (45). Briefly, tumors were mechanically disassociated into single cells, suspensions were diluted, and grown at different densities in culture media (DMEM with 10% FBS, 4.5 g/L glucose, 2 mmol/L L-glut, NEAA, and 50 μmol/L β-mercaptoethanol) until clones emerged.

Immunoprecipitation and Western blotting

For baseline MYC protein levels, total thymi from male and female 6-week–old MYC^{WT}, MYC^{T58A}, and MYC^{S62A} mice or control mice of any genotype with no Cre expression were homogenized in Ab lysis buffer (20 mmol/L Tris, pH 7.5, 50 mmol/L Nacl, 0.5% Triton X-100, 0.5% DOC, 0.5% SDS, 1 mmol/L EDTA) with protease and phosphatase inhibitors (Roche) and sonicated (Branson). Protein levels were quantified using a bicinchoninic acid (BCA) protein assay kit (Thermo Fisher Scientific) and equivalent protein levels were used to immunoprecipitate with 2 μg total MYC antibody (N262, Santa Cruz Biotechnology, catalog no. SC-764, RRID:AB_631276) or 2 μg anti-HA antibody (G036, Applied Biological Materials, RRID:AB_2801472) overnight at 4°C and then pulled down with either protein-A IPA300 beads (Repligen), or protein-G plus agarose beads (Santa Cruz Biotechnology), respectively. For detection of phosphorylated S62 MYC, tumor lysates were prepared as described above and immunoprecipitated with 2 μg anti-MYC (N262, Santa Cruz Biotechnology, catalog no. SC-764, RRID:AB_631276) overnight at 4°C and then pulled down with protein-A IPA300 beads (Repligen; refs. 44, 46). Immunoprecipitated protein was resolved via SDS-PAGE and was transferred to an Immobilon-FL PDVF membrane (Millipore). AquaBlock (EastCoast Bio) was used to block membranes. The membranes were probed with the following primary antibodies as indicated: total c-MYC antibody (Y-69, Abcam, catalog no. ab32072, RRID:AB_1191623), phosphorylated S62 MYC (33A12E10, Abcam, catalog no. ab78318, RRID:AB_10678479), and GAPDH (6C5, Thermo Fisher Scientific, catalog no. AM4300, RRID:AB_627679). Species-specific secondary antibodies conjugated to either a 680 or 800 fluorophore (LI-COR, Molecular Probes) were applied and detected with the LI-COR Odyssey Infrared Imager (LI-COR).

TCRβ deep sequencing of tumor cells and lines

Genomic DNA was extracted from tumor tissue or single cell suspensions using the DNAeasy Blood and Tissue Kit (Qiagen). Deep sequencing of the CDR3 V/J region of the T-cell receptor β (TCRβ) was performed using methods previously described (47).

RNA sequencing and gene expression analyses

RNA was extracted from previously frozen tumor tissue ($n = 3$ from each group and $n = 2$ as control) using Trizol (Invitrogen) and libraries were generated using a NEB Next Ultra Directional RNA Library Prep Kit for Illumina (NEB) per manufacturer instructions. Libraries were submitted to the OHSU Massively Parallel Sequencing Shared Resource for short read sequencing assays. Differentially expressed genes were selected with DESeq2 using an adjusted P value threshold of 0.05 and a fold change (FC) threshold

of ±1.5. Genes were further filtered using a coefficient of variation threshold of 1.0. For unsupervised hierarchical clustering, Voom normalization was performed on tumor samples using all genes and reduced to unique gene symbols, then Ward clustering was used to identify subgroups. Row scaled, hierarchically clustered heatmaps were generated using log scaled and transcripts per million (TPM) normalized values for the selected genes. Gene set enrichment analysis (GSEA) using MSigDB and ImmuneSigDB was performed to determine terms related to predominating hallmark and immune gene sets or pathways (48–50).

Data availability

The raw RNA sequencing (RNA-seq) files generated in this study can be found in the National Center for Biotechnology Information's Gene Expression Omnibus repository under the accession: GSE193995 (https://www.ncbi.nlm.nih.gov/geo/query/acc.cgi?acc=GSE193995), with token ID: ifcfccouftqvten.

Results

Thymocyte dysregulation with expression of MYC^{T58A} and MYC^{S62A}

To examine the functional roles of stabilized MYC lacking T58 phosphorylation with or without S62 phosphorylation in T-cell development and tumorigenesis, we utilized knock-in mice that conditionally express either a C-terminal HA-tagged murine MYC^{WT}, MYC with T58 mutated to Alanine (MYC^{T58A}) that has elevated S62 phosphorylation, or MYC with S62 mutated to Alanine (MYC^{S62A}) that lacks both T58 phosphorylation and S62 phosphorylation (refs. 29, 30; **Fig. 1A**). The *ROSA-Myc* knock-in mice were bred to gain one copy of *Lck-Cre* for T-cell–specific ectopic expression of homozygous RFS-*c-Myc*^{WT}, -*c-Myc*^{T58A}, or -*c-Myc*^{S62A} specifically in T cells by the double negative III (DNIII) stage of T-cell development. These mice are denoted here as MYC^{WT}, MYC^{T58A}, and MYC^{S62A} mice. PCR analysis of genomic DNA taken from various tissues at 6 weeks of age confirmed recombination of the allele primarily in thymic tissue (Supplementary Fig. S1A). Consistent with previous analysis of the RFS-*Myc* model (29, 51, 52), we found equivalent mRNA levels of ROSA promoter driven ectopic *Myc*^{WT}, *Myc*^{T58A}, and *Myc*^{S62A} mRNA expression in the three strains indicative of similar levels of recombination. This results in approximately two- to three-fold higher total *cMyc* mRNA expression in thymus tissues from the MYC^{WT}, MYC^{T58A}, and MYC^{S62A} mice as compared with no Cre controls (Supplementary Fig. S1B). As expected, based on increased MYC protein stability (Supplementary Fig. S1C), the levels of both ectopic MYC^{T58A} and MYC^{S62A} protein were about five-fold higher than the level of ectopic MYC^{WT}, despite similar mRNA levels (Supplementary Fig. S1B and S1D).

In our mice, both ectopic and endogenous MYC can heterodimerize with MAX to promote transcription of MYC target genes; moreover, MYC/MAX heterotetramers may include both ectopic and endogenous MYC (53). To determine the effects of ectopic MYC expression in the absence of endogenous MYC, C57Bl/6 mice with the *LoxP*/Cre-driven conditional deletion of endogenous *Myc* (designated $MYC^{fl/fl}$; ref. 42) were bred with the MYC^{WT}, MYC^{T58A}, and MYC^{S62A} mice. This generated new cohorts of RFS-*Myc*^{WT};*Myc*$^{fl/fl}$;*Lck-Cre*, RFS-*Myc*^{T58A};*Myc*$^{fl/fl}$;*Lck-Cre*, and RFS-*Myc*^{S62A};*Myc*$^{fl/fl}$;*Lck-Cre* mice, designated $MYC^{WT}MYC^{fl/fl}$, $MYC^{T58A}MYC^{fl/fl}$ and $MYC^{S62A}MYC^{fl/fl}$, respectively (**Fig. 1A**). All experimental mice contained only one copy of *Lck-Cre* to minimize Cre effects on T-cell development (54).

With these new cohorts, we first compared thymic weights from male and female 6-week–old mice expressing ectopic MYC with and without endogenous *Myc* to no Cre control mice. In mice with endogenous *Myc*, we found a significantly higher thymic mass in MYC^{T58A} mice as compared with control and MYC^{S62A} mice (**Fig. 1B**). Ablation of endogenous MYC significantly reduced thymic weights for all strains. $MYC^{T58A}MYC^{fl/fl}$ was capable of maintaining normal thymic weight relative to control while $MYC^{S62A}MYC^{fl/fl}$ was not. $MYC^{T58A}MYC^{fl/fl}$ thymic weights were significantly higher than $MYC^{S62A}MYC^{fl/fl}$, and both were significantly higher when compared with thymi lacking both ectopic and endogenous *Myc* expression (designated $MYC^{fl/fl}$). Overall total thymocyte numbers, composed of mainly CD4 and CD8 double-positive (DP) T cells, from all strains except MYC^{T58A} were significantly lower than control (Supplementary Fig. S2A). Further reduction in thymocyte number was seen with loss of endogenous *Myc*, with the lowest numbers of thymocytes in $MYC^{S62A}MYC^{fl/fl}$ and $MYC^{fl/fl}$ (**Fig. 1C**). Ectopic expression of MYC^{T58A} increased, and ablation of endogenous MYC decreased, spleen weight in 6-week–old mice, but ectopic MYC^{WT} and MYC^{S62A} did not have significant effects (Supplementary Fig. S2B). Total splenocyte number was also significantly higher in MYC^{T58A} mice when compared with control and MYC^{WT} mice (Supplementary Fig. S2C). This increase may be due to an early expansion of CD3-positive MYC^{T58A} T cells and loss of follicular architecture with disruption of marginal zones in the spleen (Supplementary Fig. S2D).

In addition to contributing to mitogenic cell division, MYC contributes to cell growth and can help drive apoptosis (55, 56). We did observe a significant increase in MYC^{T58A} and MYC^{S62A} DP thymocyte size (either with or without endogenous MYC) when normalized to control littermates from each strain, suggesting both unphosphorylated or phosphorylated MYC can drive increased thymocyte size in DP T cells in the thymus at 6 weeks (**Fig. 1D**; Supplementary Fig. S2A). Expression of MYC^{T58A} or MYC^{S62A} in a MYC null background did not show a loss in mature T-cell survival *ex vivo* suggesting that both can support T-cell survival programs (**Fig. 1E**; refs. 30, 43). The larger cell sizes without a loss in survival may in part support the ability of MYC^{T58A} and MYC^{S62A} to maintain thymic weight, despite having lower total thymocytes *in vivo*.

Mitogen stimulation of splenic T cells triggers cell growth through nutrient uptake and macromolecular synthesis, and the transition from quiescence to proliferation (30, 35, 57). Ectopic expression of *Myc* enhances *ex vivo* T-cell proliferation during mitogen stimulation despite a concomitant increase in apoptosis (30). To look at *ex vivo* proliferative potential of MYC^{T58A} and MYC^{S62A}, and their ability to compensate in a MYC-null background we cultured splenic T cells isolated from 6-week–old mice with the lectin Con A for 24 hours. Total BrdU incorporation of $CD4^+$ and $CD8^+$ T cells from MYC^{WT}, MYC^{T58A}, $MYC^{T58A}MYC^{fl/fl}$, MYC^{S62A}, or $MYC^{S62A}MYC^{fl/fl}$ mice were normalized to stimulated T cells from control littermates. Splenic T cells from $MYC^{S62A}MYC^{fl/fl}$ mice showed the least *ex vivo* proliferative potential compared with all other strains (**Fig. 1F**; Supplementary Fig. S2E). MYC^{T58A} T cells proliferated significantly more than MYC^{WT} T cells but this potential was lost when endogenous MYC was ablated. In general, the ablation of endogenous MYC in MYC^{T58A} and MYC^{S62A} T cells significantly diminished their *ex vivo* proliferative potential when compared with their counterparts, suggesting a cooperativity of endogenous MYC in this assay. However, unlike $MYC^{S62A}MYC^{fl/fl}$, $MYC^{T58A}MYC^{fl/fl}$ T cells maintained control levels of proliferation. Together, these data indicate that while MYC^{T58A} and MYC^{S62A} are both stabilized

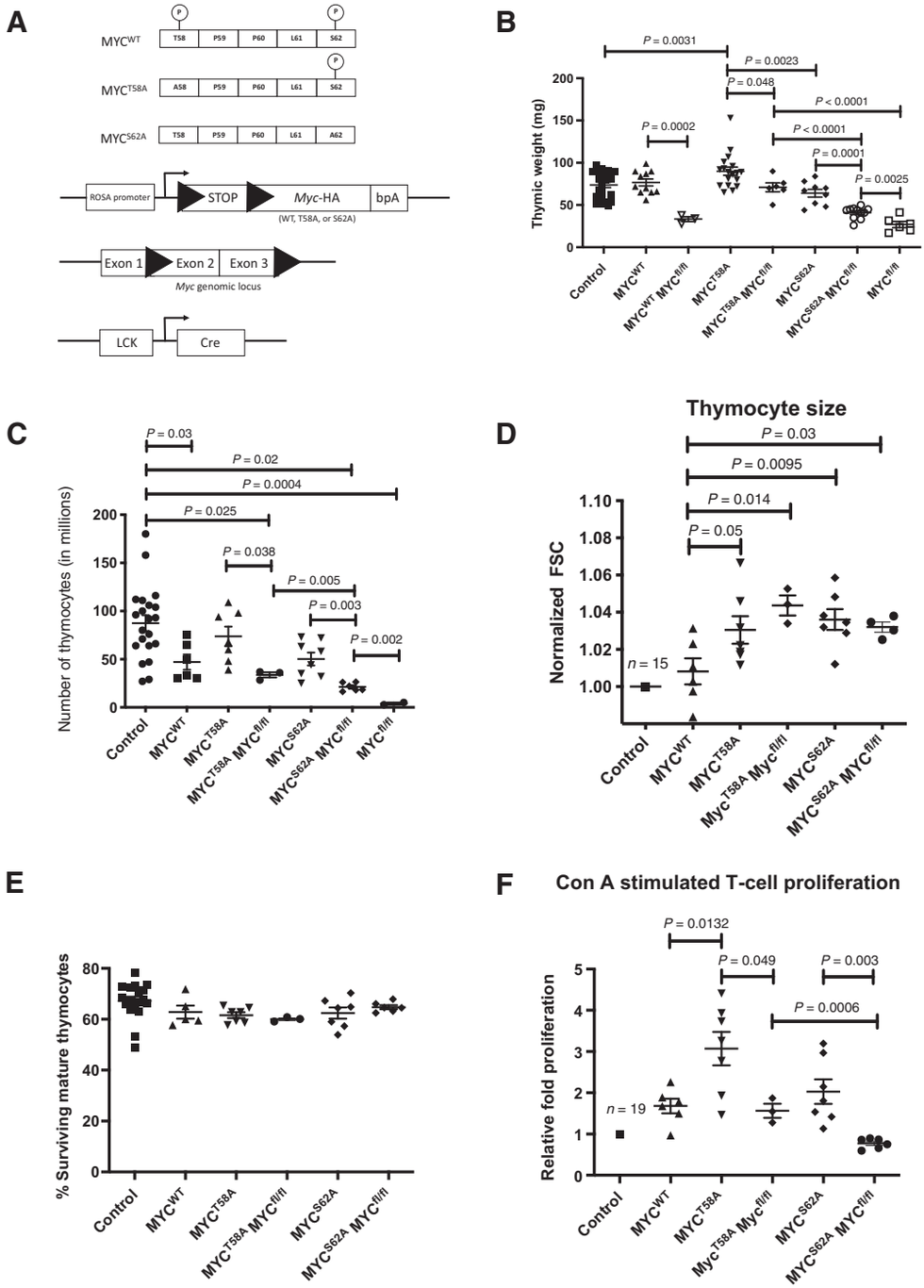

Figure 1.

Endogenous MYC is involved in thymic cellularity and *ex vivo* proliferative potential in MYC^{S62A}-expressing T cells. **A,** Schematic of MYC phosphorylation status and knock-in strategy for conditional expression of MYC^{WT}-HA, MYC^{T58A}-HA, and MYC^{S62A}-HA. Lollipop represents phosphorylation at indicated residue of MYC. Arrowheads indicate loxP sites and bpA is a transcription stop sequence. LoxP sites flank exons 2 and 3 of *Myc* at the genomic locus. Cre is driven by LCK. **B,** Thymic weight of 6-week–old mice from indicated strains ($n = 3$ or more). Error bars represent SEM. *t* tests were performed comparing thymic weight between mouse strains ($P < 0.05$ are indicated). **C,** Total number of thymocytes in 6-week–old mice from indicated strains ($n = 2$ or more). Error bars represent SEM. *t* tests were performed comparing number of thymocytes between mouse strains ($P < 0.05$ are indicated). **D,** CD4 and CD8 DP T-cell size. Cell size was determined by forward scatter area (FSC-A) and normalized to values from littermate controls ($n = 3$ or more) from indicated strains. Error bars represent SEM. *t* tests were performed comparing normalized FSC-A between mouse strains ($P \Leftarrow 0.05$ are indicated). **E,** DP T-cell *ex vivo* survival at 24 hours. Plot of CD4 and CD8 DP thymocytes from 6-week–old mice negative for Annexin V and 7AAD staining ($n = 3$ or more per strain). Error bars represent SEM. **F,** Endogenous MYC plays a role in T-cell *ex vivo* proliferative potential. Splenic $CD4^+$ and $CD8^+$ thymocytes were stimulated with 1ug of Con A for 24 hours and analyzed by FACS for BrdU incorporation ($n = 3$ or more for indicated strains). Fold increases were normalized to control littermates not expressing *Lck*-Cre. Error bars represent SEM. *t* tests were performed comparing relative fold proliferation between mouse strains ($P < 0.05$ are indicated).

and expressed at similar higher levels compared with MYC^{WT}, only MYC^{T58A} mice showed significant difference in thymic and splenic mass, cell count, cell size, and *ex vivo* proliferative potential when compared with control mice with no *Lck*-Cre expression, and with endogenous *Myc* loss, MYC^{T58A} was mostly able to maintain control levels of these metrics while MYC^{S62A} was not.

Lymphomagenesis latency and penetrance is different in MYC^{T58A} versus MYC^{S62A} mice

Following our 6-week studies on the different MYC strains we conducted survival studies. Overall survival of MYC^{T58A} mice with or without endogenous MYC was significantly shortened when compared with all other strains including control mice. Interestingly,

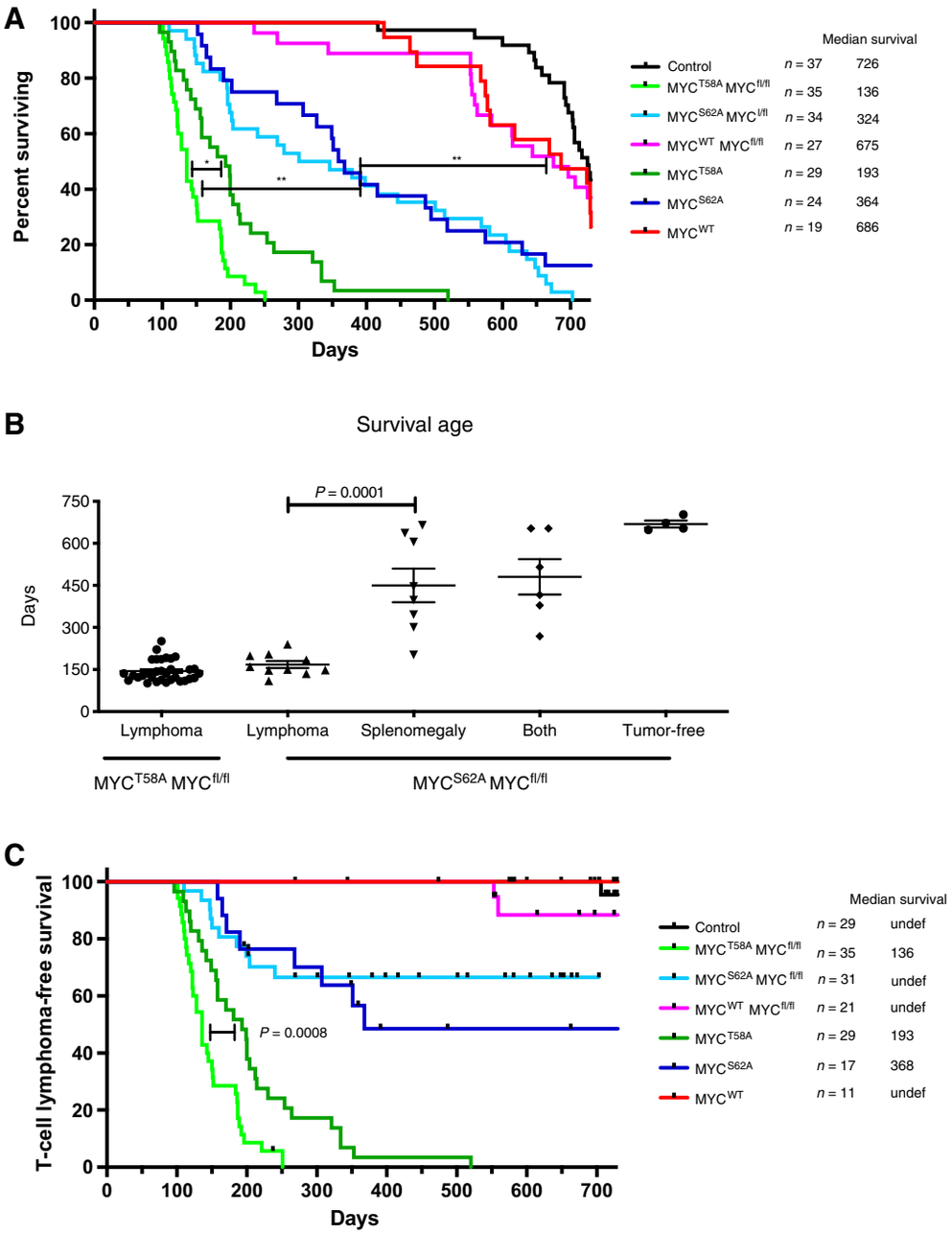

Figure 2.
Ablation of endogenous MYC decreases the latency of lymphomagenesis in MYC^{T58A} mice and does not prevent lymphomagenesis in MYC^{S62A} mice. **A,** Kaplan–Meier curve of percentage of surviving mice expressing MYC^{WT}, MYC^{T58A}, or MYC^{S62A} in T cells with or without endogenous MYC (denoted $MYC^{fl/fl}$) with strains ($n = 19$ or more) and median survival in days as indicated. Significance was determined with a log-rank test, (*, $P = 0.0004$; **, $P < 0.0001$). **B,** Breakdown of tumor-type by survival age ($n = 4$ or more). Error bars represent SEM. *t* tests were performed comparing tumor phenotype between mouse strains ($P < 0.05$ is indicated). **C,** Kaplan-Meier curve of T-cell lymphoma-free survival of mice expressing MYC^{WT}, MYC^{T58A}, or MYC^{S62A} in T cells with or without endogenous MYC (denoted $MYC^{fl/fl}$) with strains ($n = 11$ or more) and median survival in days as indicated. Only mice presenting with T-cell lymphoma and no splenomegaly were included in the curve. Significance was determined with a log-rank test, ($P < 0.05$ is indicated). undef, undefined.

survival of $MYC^{T58A}MYC^{fl/fl}$ mice was significantly shorter than syngeneic MYC^{T58A} mice (136 days and 193 days, respectively), suggesting that the expression of endogenous *Myc* dampens the tumorigenic activity of Myc^{T58A} *in vivo*. Median overall survival of MYC^{S62A} and $MYC^{S62A}MYC^{fl/fl}$ mice was significantly longer than the MYC^{T58A} cohort (364 and 324 days, respectively), but significantly shorter than MYC^{WT} mice (**Fig. 2A**). Median survival of both $MYC^{WT}MYC^{fl/fl}$ and MYC^{WT} mice were 675 days and 686 days, respectively. The survival curve data suggests that expression of MYC^{WT} in the presence or absence of endogenous MYC has a very low tumorigenic penetrance in our model where total *Myc* expression is only approximately two- to three-fold above endogenous levels (Supplementary Fig. S1B; ref. 29). This cohort did not show any significant difference in survival when compared with control mice not expressing *Lck*-Cre.

Necropsies of moribund mice revealed thymic lymphomas developed in MYC^{T58A} and $MYC^{T58A}MYC^{fl/fl}$ mice with 100% penetrance. A similar presentation of thymic lymphomas occurred in some MYC^{S62A} and $MYC^{S62A}MYC^{fl/fl}$ mice, but necropsy also revealed a high prevalence of splenomegaly in the MYC^{S62A} and $MYC^{S62A}MYC^{fl/fl}$ mice that in some mice cooccurred with an enlarged thymus (hereafter, thymic mass) with unconfirmed etiology due to the presence of splenomegaly and these mice showed similar survival ages compared with the same strain of mice with only splenomegaly (395 and 450 days, respectively) (Supplementary Fig. S3A; **Fig. 2B**; and **Table 1**). In contrast, $MYC^{T58A}MYC^{fl/fl}$ and $MYC^{S62A}MYC^{fl/fl}$ mice that developed thymic lymphomas without evidence of splenomegaly had significantly shorter but similar survival ages (144 and 168 days, respectively) indicating the lethality of a rapidly expanding lymphoma. Thus, despite the decrease in *ex vivo* proliferative potential in $MYC^{S62A}MYC^{fl/fl}$ T cells, reduction in thymic weight and thymocyte number, $MYC^{S62A}MYC^{fl/fl}$ mice can develop thymic lymphomas, but at a substantially lower penetrance (~36%) than MYC^{T58A} and $MYC^{T58A}MYC^{fl/fl}$ mice (**Fig. 2C**; **Table 1**). Together, this indicates that $MYC^{S62A}MYC^{fl/fl}$ mice can spontaneously develop thymic lymphomas, however if they escape early thymic lymphoma development, they either succumb to splenomegaly with or without a thymic mass, or persist tumor free (**Fig. 2B–C**; **Table 1**).

Thymic lymphomas from $MYC^{T58A}MYC^{fl/fl}$ and $MYC^{S62A}MYC^{fl/fl}$ mice are predominantly T cells while thymic masses with splenomegaly in $MYC^{S62A}MYC^{fl/fl}$ mice are B-cell lymphomas

Tumor tissue from $MYC^{T58A}MYC^{fl/fl}$ and $MYC^{S62A}MYC^{fl/fl}$ mice with only thymic lymphomas were histologically similar. These thymic lymphomas were relatively homogenous lymphocytic infiltrates in the thymic compartments with disrupted architectures and were categorized as T-cell lymphomas by cytopathology analysis performed by a hematopathologist (**Fig. 3A**; Supplementary Table S3). In contrast, the predominant cells in thymic masses that cooccurred with splenomegaly in $MYC^{S62A}MYC^{fl/fl}$ mice had greater cytoplasm:nucleus ratios, irregular nuclei, and showed B-cell plasmacytic infiltrates which were characterized as malignant B-cell lymphomas (**Fig. 3B**; Supplementary Fig. S3B; and Supplementary Table S3). These thymic masses were further characterized by IF to show heterogeneous populations of CD45R (B220)– and CD3-positive cells ($CD3^+$) unlike cells in thymic lymphomas from $MYC^{T58A}MYC^{fl/fl}$ and $MYC^{S62A}MYC^{fl/fl}$ mice, which were almost entirely $CD3^+$ T cells (**Fig. 3C**). We developed a flow cytometry panel capable of identifying T cells at varying stages of development (**Table 2**; Supplementary Table S4; and Supplementary Fig. S4A). All ten $MYC^{T58A}MYC^{fl/fl}$ and two $MYC^{S62A}MYC^{fl/fl}$ thymic lymphomas analyzed were 80% to 100% $Thy1.2^+$, confirming they were T-cell lymphomas. Eight tumors contained primarily $CD4^+$ $CD8^+$ DP thymocytes (**Table 2**; Supplementary Fig. S4B). $MYC^{T58A}MYC^{fl/fl}$ tumors H128 and H520 each contained approximately 45% DP thymocytes and 40% to 50% $CD4^+$ single-positive (SP) thymocytes, suggesting about half of the tumor cells had progressed past the DP stage. Tumor H204 was $CD4^+$ SP, the most differentiated phenotype among $MYC^{T58A}MYC^{fl/fl}$ tumors. $MYC^{T58A}MYC^{fl/fl}$ tumor H144 was at the earliest stage of development, as 26% of cells were $CD4^-$ and $CD8^-$ double-negative (DN), primarily DN4 (**Table 2**; Supplementary Fig. S4C), while the remaining cells were primarily $CD8^+$, most likely $CD8^+$ immature SP (ISP) thymocytes (58). Altogether, these data indicate that $MYC^{T58A}MYC^{fl/fl}$ and $MYC^{S62A}MYC^{fl/fl}$ thymic lymphomas represent T-ALL tumors at various stages of T-cell development (**Table 2**; Supplementary Table S4).

As described above, mice expressing the MYC^{S62A} mutation sometimes developed T-cell lymphomas, but other times developed splenomegaly (**Table 1**), with thymic masses being primarily B220-positive (**Fig. 3C**), suggesting a B-cell lineage. We developed a flow cytometry panel that could distinguish B1 B cells, B2 marginal zone B cells, B2 follicular B cells, and plasma cells (59, 60), and a panel to identify other immune cell types and applied them to thymic masses cooccurring with splenomegaly in $MYC^{S62A}MYC^{fl/fl}$ mice (**Table 2**; Supplementary Table S4; and Supplementary Figs. S5A and S6). $MYC^{S62A}MYC^{fl/fl}$ tumor I442 expressed IgD and CD23, consistent with B2 follicular B cells (**Table 2**; Supplementary Fig. S5B). $MYC^{S62A}MYC^{fl/fl}$ tumors I259 and I411 lacked surface immunoglobulin (not shown) but were

Table 1. Summary of phenotypes from necropsied cohorts of mice.

Strain	T-cell lymphoma only	Splenomegaly only	Splenomegaly and thymic mass	Neither by 650 days
Myc^{WT} $Myc^{fl/fl}$ $n = 20$	1 (5%)	2 (10%)	1 (5%)	16 (80%)
Myc^{WT} $n = 10$	0	3 (30%)	0	7 (70%)
Myc^{T58A} $Myc^{fl/fl}$ $n = 34$	34[a,b] (100%)	0	0	0
Myc^{T58A} $n = 13$	13 (100%)	0	0	0
Myc^{S62A} $Myc^{fl/fl}$ $n = 28$	10[c] (36%)	9[d,e] (32%)	5 (18%)	4 (14%)
Myc^{S62A} $n = 13$	8 (62%)	3 (23%)	0	2 (15%)

Note: Cohorts of mice were monitored until moribund. Numbers for each phenotype at time of necropsy are reported for mice with a thymic lymphoma, splenomegaly, splenomegaly and thymic mass, or no signs of a mass by 650 days (percentage in parentheses). Significance reported by performing Fisher exact test comparing tumor phenotypes between two mouse strains.

[a]Indicates $P < 0.0001$ comparing T-cell lymphoma only between $MYC^{WT}MYC^{fl/fl}$ and $MYC^{T58A}MYC^{fl/fl}$.

[b]Indicates $P < 0.0001$ comparing T-cell lymphoma only between $MYC^{T58A}MYC^{fl/fl}$ and $MYC^{S62A}MYC^{fl/fl}$.

[c]Indicates $P = 0.0156$ comparing T-cell lymphoma only between $MYC^{WT}MYC^{fl/fl}$ and $MYC^{S62A}MYC^{fl/fl}$.

[d]Indicates $P = 0.0159$ comparing splenomegaly with or without thymic mass between $MYC^{T58A}MYC^{fl/fl}$ and $MYC^{S62A}MYC^{fl/fl}$.

[e]Indicates $P < 0.0001$ comparing splenomegaly with or without thymic mass between $MYC^{T58A}MYC^{fl/fl}$ and $MYC^{S62A}MYC^{fl/fl}$.

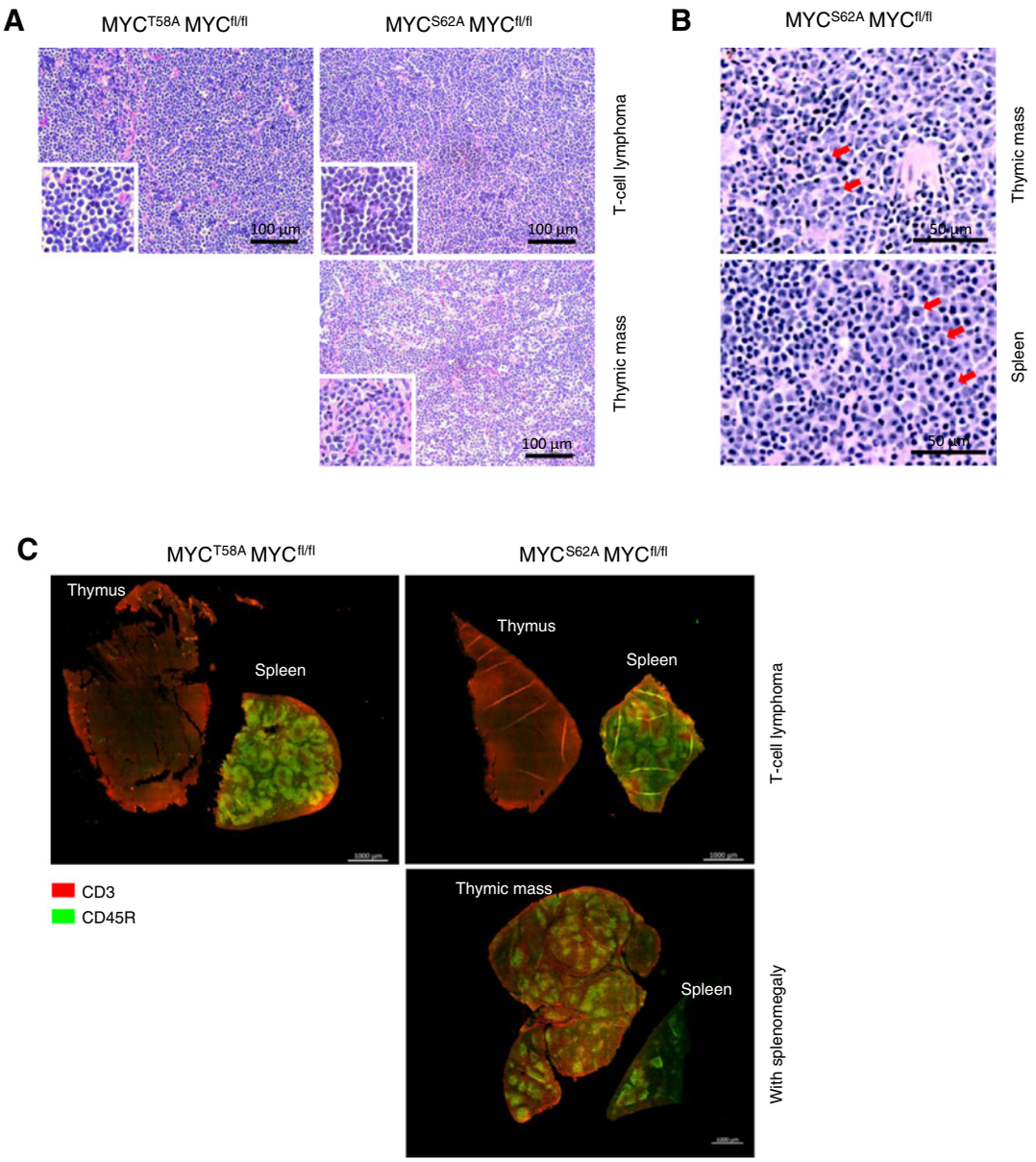

Figure 3.

T-cell lymphomas from MYC^{T58A}MYC$^{fl/fl}$ and MYC^{S62A}MYC$^{fl/fl}$ mice are histologically similar while thymic masses from MYC^{S62A}MYC$^{fl/fl}$ mice with splenomegaly are B-cell lymphomas. **A,** H&E staining of T-cell lymphomas from MYC^{T58A}MYC$^{fl/fl}$ and MYC^{S62A}MYC$^{fl/fl}$ mice. Top panel: Representative images from mice with only T-cell lymphomas (40x; $n = 3$ or more). Bottom left, Representative image of thymic mass from mouse with splenomegaly (40x; $n = 3$ or more). Insets are 60x magnification. **B,** Representative images of thymic mass and spleen from mouse with splenomegaly. Plasma cells indicated by red arrows. **C,** CD45R^{+} B cells in a thymic mass from MYC^{S62A}MYC$^{fl/fl}$ mice with splenomegaly. Top, Representative images of paraffin-embedded, formalin-fixed thymi and spleens as indicated from MYC^{T58A}MYC$^{fl/fl}$ and MYC^{S62A}MYC$^{fl/fl}$ mice stained by IF for either CD3^{+} (red) and CD45R^{+} (green) cells (20x; $n = 3$ or more). Bottom left, Representative image from MYC^{S62A}MYC$^{fl/fl}$ mouse with thymic mass and splenomegaly [CD3^{+} (red) and CD45R^{+} (green) cells (20x)] ($n = 3$ or more).

CD138^{+} and thus identified as plasma cells (**Table 2**; Supplementary Fig. S5C). Interestingly, MYC^{S62A}MYC$^{fl/fl}$ tumors I86 and I440 expressed B220 and/or CD19, consistent with tumors of a B-cell lineage, but lacked any other B-cell subset markers (**Table 2**). While a significant fraction of I86 and I440 cells were T cells, these were likely normal mature CD4 and CD8 T cells trafficking through the spleen, and relatively few cells in any sample were identified as myeloid or natural killer (NK) cells (Supplementary Table S4; Supplementary Fig. S6). Histology indicated a starry sky appearance for I440, a hallmark of Burkitt lymphoma (Supplementary Fig. S3B), and consistent with the lack of B1, B2, and plasma cell markers.

Table 2. Summary of lymphoma analyzed by FACS show T cells in thymic lymphomas and B cells in thymic masses with splenomegaly.

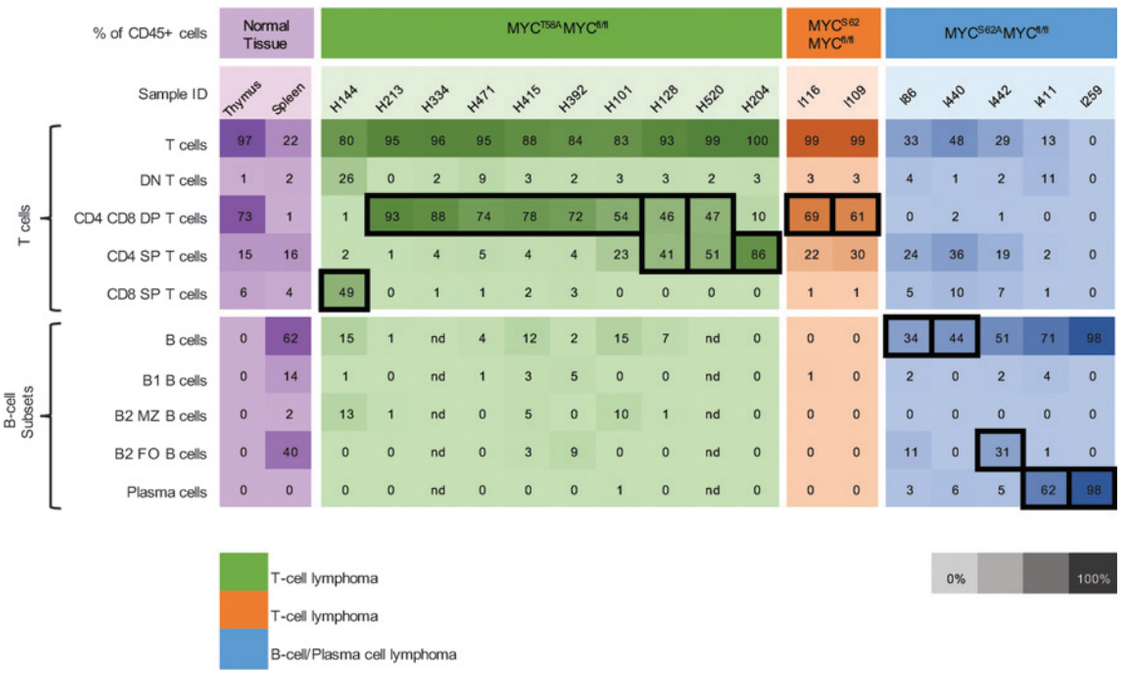

Note: The indicated MYC^{T58A}MYC$^{fl/fl}$ and MYC^{S62A}MYC$^{fl/fl}$ tumors were analyzed by FACS. Among CD45^{+} cells, percentages of T-cell and B-cell subsets are shown. Not all columns add up to 100% due to rounding. Proportions found in normal control spleen and thymus are shown for comparison. Gating schemes and complete subset data are provided in Supplementary Table S4; Supplementary Figs. S4–S6.
Abbreviation: nd, not determined.

MYC^{S62A} can drive clonal T-cell lymphomas

To further validate the ability of MYC^{S62A} to drive T-cell lymphoma in a MYC$^{fl/fl}$ background, we first tested if deletion of endogenous *Myc* was complete. *Lck*-Cre–mediated recombination can be variable and incomplete in T cells (61) and the concern was that tumor forming T cells may be from a subset population that have escaped Cre-mediated recombination of endogenous *Myc*. Thus, we measured *Myc* mRNA and protein levels from several T-cell lymphomas from both MYC^{T58A}MYC$^{fl/fl}$ and MYC^{S62A}MYC$^{fl/fl}$ mice (n = 5 from each strain; **Fig. 4A** and **B**). The mRNA levels of endogenous *Myc* in the T-cell lymphomas from both MYC^{T58A}MYC$^{fl/fl}$ and MYC^{S62A}MYC$^{fl/fl}$ mice were significantly lower when normalized to control thymi from any genotype with no Cre expression, consistent with deletion of endogenous MYC in the models, while expression of ectopic message was equivalently high in both knock-in strains (**Fig. 4A**). In addition, pS62 MYC was only detected in MYC^{T58A}MYC$^{fl/fl}$ and not MYC^{S62A}-MYC$^{fl/fl}$ T-cell lymphomas and generated lymphoma cell lines (**Fig. 4B** and **C**). Likewise, CD3^{+} cells in MYC^{T58A}MYC$^{fl/fl}$ T-cell lymphomas stained robustly for pS62 MYC, unlike MYC^{S62A}MYC$^{fl/fl}$, which showed little pS62 MYC staining in CD3^{+} cells; although pS62 MYC was strongly detected in the CD45R-positive (CD45R^{+}) cells in thymic masses from MYC^{S62A}MYC$^{fl/fl}$ mice with splenomegaly (**Fig. 4D**). Taken together, these data indicate that the T cells in MYC^{S62A}MYC$^{fl/fl}$ tumors do not express endogenous *Myc* and that this mutant form of MYC lacking phosphorylation at T58 and S62 is capable of driving T-cell lymphoma in our model, albeit at a lower penetrance.

MYCN is essential in early DN stages of T-cell development but decreases in the late DN stage as MYC expression increases (62). However, MYCN can substitute for MYC during embryogenesis (63), and can drive indolent B-cell lymphomas (64). We hypothesized that MYCN was playing a role in MYC^{S62A}MYC$^{fl/fl}$ T-cell lymphomagenesis however, analysis of mRNA levels of *Mycn* in these T-cell lymphomas revealed low levels of expression compared with control thymi, decreasing the likelihood of an oncogenic compensatory role by MYCN in T-cell lymphomagenesis in the MYC^{S62A}MYC$^{fl/fl}$ model (Supplementary Fig. S7A). Although *Mycn* mRNA expression was variable among MYC^{S62A}MYC$^{fl/fl}$ tumors, it was not significantly higher than in MYC^{T58A}MYC$^{fl/fl}$ tumors.

B1 cells, a subclass of B cells have been reported to express *Lck* (65–67), which could lead to leaky ectopic MYC expression in the spleen in our model (Supplementary Fig. S1A). To address whether this was accounting for the B-cell expansion in MYC^{S62A}-MYC$^{fl/fl}$ mice that develop splenomegaly and B-cell lymphomas, we looked at the number of copies of HA-tag *Myc* mRNA from RNA sequence data of thymic masses from MYC^{S62A}MYC$^{fl/fl}$ mice accompanied with splenomegaly compared with MYC^{S62A}-MYC$^{fl/fl}$ and MYC^{T58AA}MYC$^{fl/fl}$ mice that had T-cell lymphoma (**Fig. 4E**). Ectopic *Myc*-HA-tag mRNA levels in thymic masses from MYC^{S62A}MYC$^{fl/fl}$ mice with splenomegaly was not significantly higher than control thymi without the *Lck*-Cre transgene, confirming that these malignant B cells infiltrate the thymi without expressing ectopic *Myc*^{S62A} and consistent with their robust pS62 MYC staining (**Fig. 4D**).

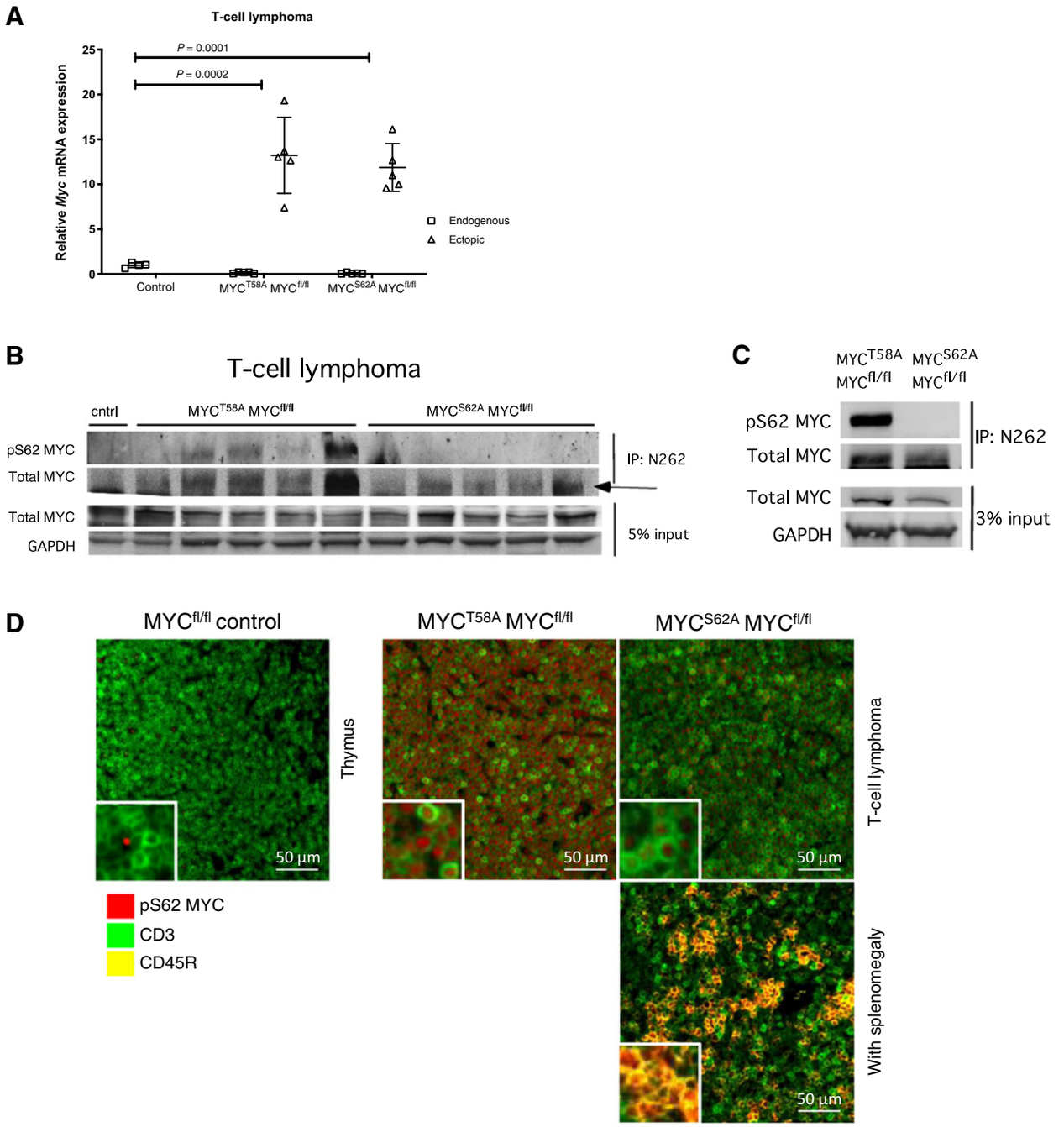

Figure 4.

$MYC^{S62A}MYC^{fl/fl}$ mice not expressing endogenous *Myc* are capable of developing clonal T-cell lymphomas. **A,** *Myc* mRNA levels in T-cell lymphomas. RNA was extracted cDNA generated from T-cell lymphomas or normal thymic tissue. *Myc* endogenous and ectopic levels were assessed by qRT-PCR ($n = 5$ from each group). CT values were normalized to *Tbp* and relative expression normalized to control thymi. Error bars represent SEM. *t* tests were performed comparing endogenous *Myc* levels between control and $MYC^{T58A}MYC^{fl/fl}$ or $MYC^{S62A}MYC^{fl/fl}$ mice ($P < 0.05$ are indicated). **B,** Phosphorylated S62 MYC protein in T-cell lymphomas. Tumor lysates were immunoprecipitated with the total MYC antibody N262 and probed with a phospho-S62 MYC specific antibody and the total MYC antibody Y69. GAPDH was used as a loading control from 5% of the input lysate. Arrow indicates the total MYC protein band above a nonspecific IgG heavy chain band. **C,** Phosphorylated S62 MYC protein status in clonal T-cell lymphoma cell lines from $MYC^{T58A}MYC^{fl/fl}$ and $MYC^{S62A}MYC^{fl/fl}$ mice. Phosphorylated S62 MYC protein was assayed by immunoprecipitating with the total MYC protein antibody N262 in cell lines derived from T-cell lymphomas from $MYC^{T58A}MYC^{fl/fl}$ and $MYC^{S62A}MYC^{fl/fl}$ mice. Blot was probed with a phospho-S62 MYC specific antibody and total MYC antibody Y69. GAPDH was used as a loading control from 3% of input lysate. **D,** Phosphorylated S62 MYC in $CD3^+$ T-cells. Representative IF staining of thymic tissue from a $MYC^{fl/fl}$ control thymus, a T-cell lymphoma from $MYC^{T58A}MYC^{fl/fl}$ and $MYC^{S62A}MYC^{fl/fl}$ mice, and a $MYC^{S62A}MYC^{fl/fl}$ mouse with splenomegaly. Staining for pS62 MYC (red), CD3 (green), and CD45R (yellow; 10x; $n = 2$ or more). Insets are 50× magnification. (*Continued on the following page.*)

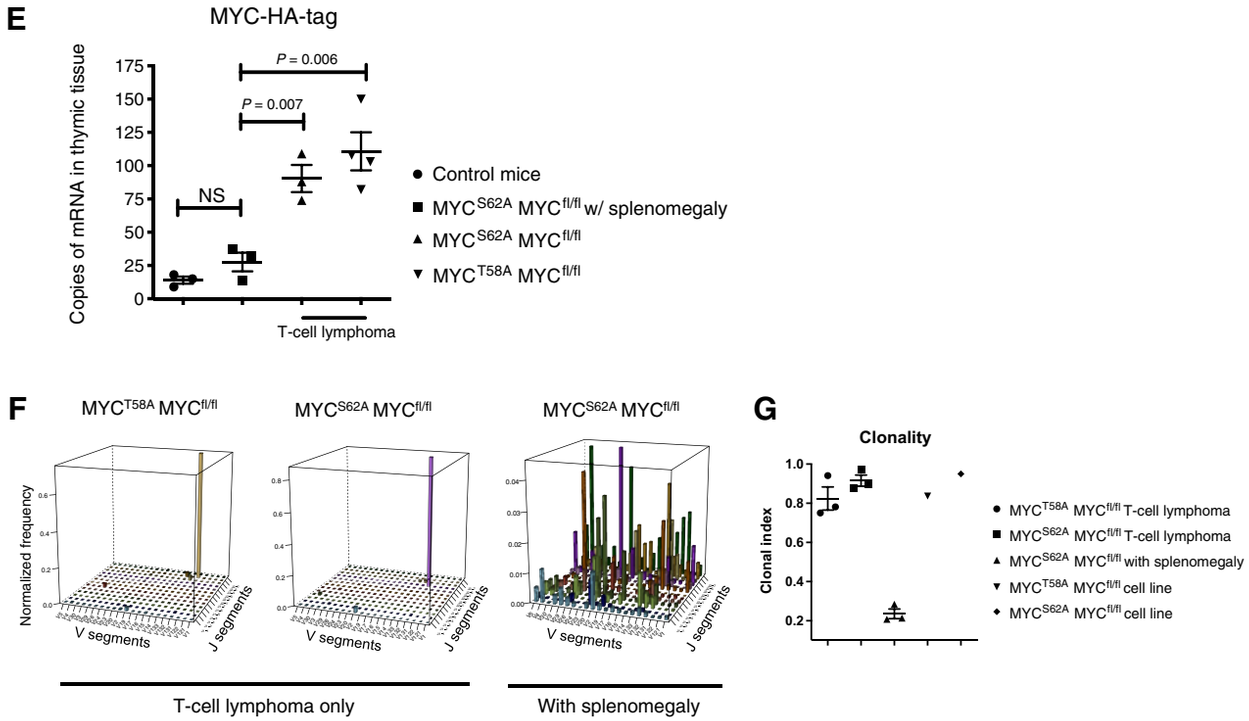

Figure 4.

(*Continued.*) **E,** Number of copies of mRNA with a MYC-HA-tag sequence associated with ectopic *Myc* expression was plotted from RNA sequence data from T-cell lymphomas or thymic mass with splenomegaly, and control ($n = 3$ or more) indicating expression level of ectopic *Myc*. Error bars represent SEM. *t* tests were performed comparing mRNA levels ($P < 0.05$ are indicated). **F,** T-cell lymphomas from $MYC^{T58A}MYC^{fl/fl}$ and $MYC^{S62A}MYC^{fl/fl}$ mice without splenomegaly are clonal. Deep sequencing of the CDR3 V/J region of the TCRβ was performed on thymic tissue ($n = 3$ for each indicated group) and tumor cell lines ($n = 1$ from indicated group). Representative 3D bar graphs with a single bar or multiple bars reflect a monoclonal or polyclonal repertoire of TCRβ respectively. **G,** Dot plot summarizing clonal index of TCRβ repertoire from indicated strains ($n = 3$ for each tumor type) and cell lines ($n = 1$ for each strain). Error bars represent SEM. Clonal index close to 1 indicate a monoclonal repertoire of TCRβ. Cntrl, control; IP, immunoprecipitation; NS, not significant.

Sequencing of the CDR3 V/J region of the TCR ($n = 3$ for each tumor phenotype) from thymic tumor tissue were predominantly clonal in T-cell lymphomas from both $MYC^{T58A}MYC^{fl/fl}$ and $MYC^{S62A}MYC^{fl/fl}$ mice compared with a more diverse population of T- and B-cells in $MYC^{S62A}MYC^{fl/fl}$ thymic masses with accompanying splenomegaly (**Fig. 4F**; ref. 47). When comparing clonality indexes, the T-cell lymphomas in $MYC^{T58A}MYC^{fl/fl}$ and $MYC^{S62A}MYC^{fl/fl}$ mice, as well as cell lines derived from representative T-cell lymphomas showed clonality while $MYC^{S62A}MYC^{fl/fl}$ thymic masses with splenomegaly did not (**Fig. 4G**). Together, these results indicate that malignant B cells infiltrating into the thymic cavity underlie the appearance of thymic lymphomas in the $MYC^{S62A}MYC^{fl/fl}$ mice with splenomegaly; and this infiltration is not originating from cells with MYC^{S62A} transgene expression. This is consistent with the longer life span of mice in which transgene-driven T-cell lymphoma is not the cause of mouse study endpoint. Taking this into consideration reveals that the difference in penetrance of T-cell lymphoma between the $MYC^{T58A}MYC^{fl/fl}$ and $MYC^{S62A}MYC^{fl/fl}$ mice is stark (**Fig. 2C**).

T-cell lymphomas from $MYC^{T58A}MYC^{fl/fl}$ and $MYC^{S62A}MYC^{fl/fl}$ mice show distinct pathway enrichment

Clonal T-cell expansion is a hallmark of T-cell lymphomas in $MYC^{T58A}MYC^{fl/fl}$ and $MYC^{S62A}MYC^{fl/fl}$ mice without splenomegaly. To determine if similar gene expression profiles are present in the T-cell lymphomas in the $MYC^{T58A}MYC^{fl/fl}$ and $MYC^{S62A}MYC^{fl/fl}$ mice, we used bulk RNA-sequencing data of tissue from T-cell lymphomas from $MYC^{T58A}MYC^{fl/fl}$ and $MYC^{S62A}MYC^{fl/fl}$ mice, as well as from thymic masses in $MYC^{S62A}MYC^{fl/fl}$ mice with accompanying splenomegaly. Unsupervised hierarchical clustering of the RNA-seq data ($n = 9$) resulted in three distinct groups, with T-cell lymphomas from $MYC^{T58A}MYC^{fl/fl}$ and $MYC^{S62A}MYC^{fl/fl}$ mice clustering separately, but closer together than thymic masses with splenomegaly from $MYC^{S62A}MYC^{fl/fl}$ mice (**Fig. 5A**). Distinct clustering between $MYC^{T58A}MYC^{fl/fl}$ and $MYC^{S62A}MYC^{fl/fl}$ T-cell lymphomas was also seen with immunologic gene sets when performing analysis using the ImmuneSigDB gene set (Supplementary Fig. S7B; ref. 50), suggesting the different forms of mutant MYC drove transcriptionally distinct tumors. Visualization of differentially regulated genes between $MYC^{T58A}MYC^{fl/fl}$ and $MYC^{S62A}MYC^{fl/fl}$ T-cell lymphomas with an adjusted *P* value cut-off point of 0.05 and FC cut-off point of ± 1.5 revealed 486 genes (**Fig. 5B**; Supplementary Table S5). Performing GSEA with the Hallmarks of Cancer gene sets revealed the T-cell lymphomas from $MYC^{T58A}MYC^{fl/fl}$ mice were enriched for genes involved in KRAS signaling, angiogenesis, and IFNα response (**Fig. 5C**; Supplementary Table S6). Interestingly, $MYC^{S62A}MYC^{fl/fl}$ T-cell lymphomas were enriched for gene sets involved in the G_2–M checkpoint, MYC, and

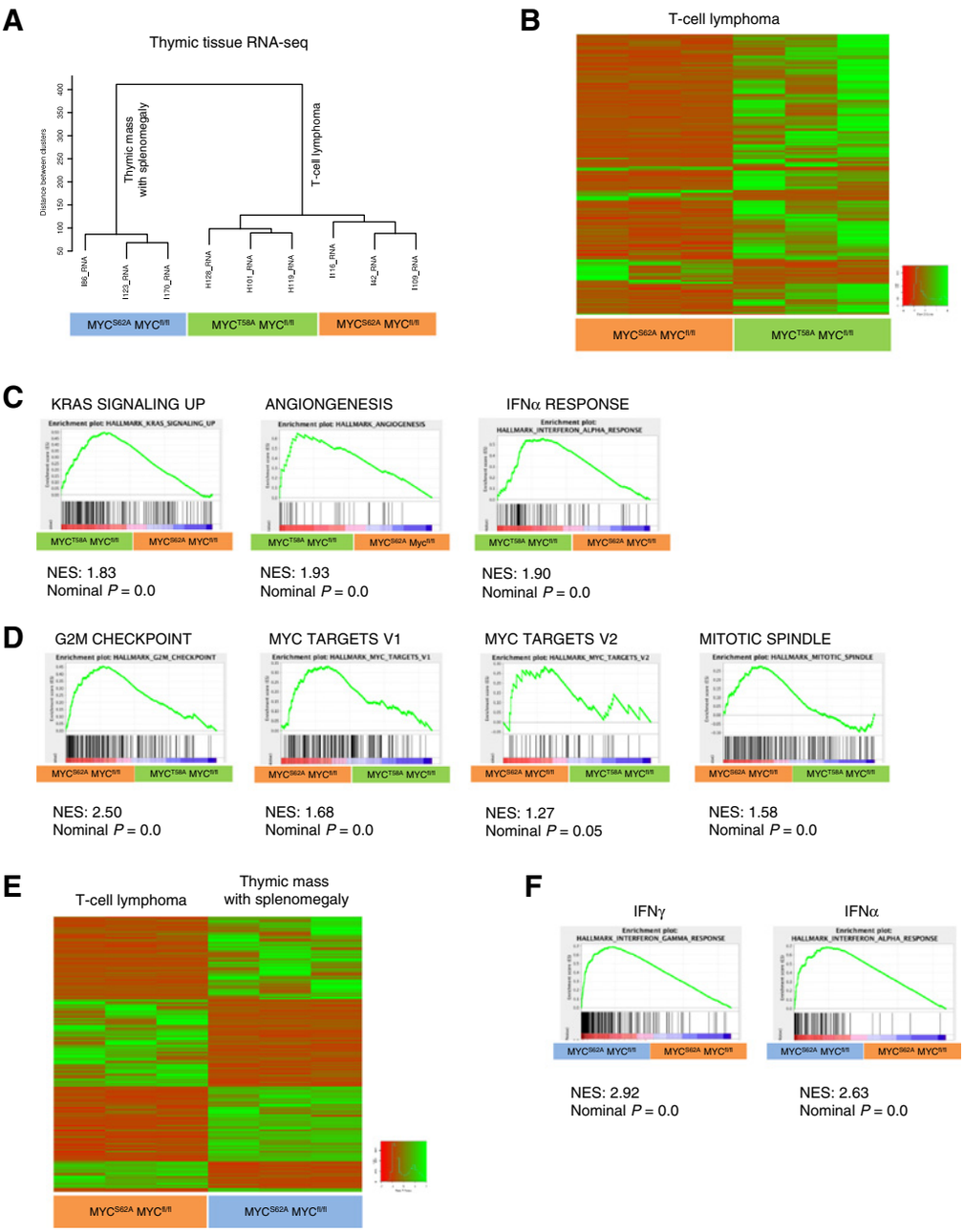

Figure 5.
T-cell lymphomas from $MYC^{T58A}MYC^{fl/fl}$ and $MYC^{S62A}MYC^{fl/fl}$ mice show distinct pathway enrichment. **A,** Unsupervised hierarchical Ward clustering of nine thymic tissue from $MYC^{T58A}MYC^{fl/fl}$ and $MYC^{S62A}MYC^{fl/fl}$ mice by RNA-seq gene expression. Three clusters emerged as indicated. **B,** Heatmap of T-cell lymphomas from $MYC^{T58A}MYC^{fl/fl}$ and $MYC^{S62A}MYC^{fl/fl}$ mice ($n = 3$ for each indicated group) with an adjusted *P* value cut-off point of 0.05 and FC cut-off point of ± 1.5. **C,** Top enriched genesets in $MYC^{T58A}MYC^{fl/fl}$ T-cell lymphomas. GSEA comparing T-cell lymphomas from $MYC^{T58A}MYC^{fl/fl}$ to $MYC^{S62A}MYC^{fl/fl}$ mice. **D,** Top enriched gene sets in $MYC^{S62A}MYC^{fl/fl}$ T-cell lymphomas. GSEA was performed comparing RNA-seq data of T-cell lymphomas from $MYC^{S62A}MYC^{fl/fl}$ to $MYC^{T58A}MYC^{fl/fl}$ mice. **E,** Heatmap of thymic mass and T-cell lymphoma from $MYC^{S62A}MYC^{fl/fl}$ mice with or without splenomegaly respectively ($n = 3$ for each indicated group) with an adjusted *P* value cut-off point of 0.05 and FC cut-off point of ± 1.5. **F,** Top enriched gene sets in $MYC^{S62A}MYC^{fl/fl}$ thymic mass with splenomegaly. GSEA was performed comparing RNA-seq data of thymic tissue from $MYC^{S62A}MYC^{fl/fl}$ mice with or without splenomegaly. NES, normalized enrichment scale.

mitotic spindle, consistent with a potential role of genomic instability in tumor progression for the MYC^{S62A} mutant as was previously observed (ref. 29; **Fig.5D**; Supplementary Table S6). Taken together, these data suggest that these two mutant forms of MYC may drive T-cell lymphomas through mechanistically different pathways.

We found 1,747 differentially regulated genes between thymic masses from $MYC^{S62A}MYC^{fl/fl}$ mice with splenomegaly versus T-

cell lymphomas from $MYC^{S62A}MYC^{fl/fl}$ (**Fig. 5E**; Supplementary Table S7) with an adjusted *P* value cut-off point of 0.05 and FC cut-off point of ±1.5. The thymic masses with splenomegaly showed enrichment of IFNα and γ gene sets (**Fig. 5F**; Supplementary Table S7), which may be due to the infiltration of malignant B cells.

Discussion

MYC protein levels are found to be constitutively high in human tumors and play a role in tumorigenic activity. High MYC levels can activate both apoptosis and proliferation pathways and are also associated with genomic instability. MYC protein levels are affected by stability, which is regulated by phosphorylation at T58 and S62, and dysregulation of phosphorylation at these sites is often associated with cancer (29, 68). By using the constitutive but relatively weak ROSA promoter, we were able to express *c-Myc* phosphorylation mutant mRNA at near physiologic levels. This allowed us to investigate the effects of phosphorylation at these sites *in vivo*, particularly the MYC^{S62A} mutant, the activity of which has been poorly understood with conflicting reports including reduced transforming activity *in vitro*, contribution to genomic instability *in vivo*, and the presence of MYC^{T58I} mutations in Burkitt lymphoma that similarly lacks T58 and S62 phosphorylation (7, 24, 26, 29). We used the *Lck*-Cre model of recombination, since this occurs as earlier as the DN2 stage of T-cell differentiation (41, 69) and therefore allowed us to perturb an *in vivo* developmental process involving stages of proliferation, differentiation, and apoptosis.

Consistent with a reduced function of the MYC^{S62A} mutant, we found that thymic weight and number of thymocytes in $MYC^{S62A}MYC^{fl/fl}$ mice was significantly reduced, although higher than the $MYC^{fl/fl}$ mice, indicating some activity of this mutant on its own. Further, the proliferative potential of $MYC^{S62A}MYC^{fl/fl}$ splenic T cells *ex vivo* showed a substantial decrease relative to littermate control levels when exposed to the mitogen Con A indicating that MYC^{S62A} has a poor capacity to drive acute proliferation in response to these mitogenic signals in the absence of endogenous MYC. However, despite these deficiencies, $MYC^{S62A}MYC^{fl/fl}$ mice developed T-cell lymphomas histologically similar to $MYC^{T58A}MYC^{fl/fl}$ mice, although at a substantially lower penetrance. We found that these T-cell lymphomas resembled human T-ALL tumors by flow cytometry. Most lymphomas expressed CD4 and CD8, indicating that DP thymocytes were the most likely cell of origin. These tumors were clonal and did not show escape from endogenous *Myc* ablation or strong compensation by *Mycn*. While 36% of $MYC^{S62A}MYC^{fl/fl}$ mice developed these T-cell lymphomas and 14% remained tumor free to study endpoint, approximately 50% of necropsied mice succumbed to splenomegaly with or without an accompanying thymic mass. Thymic masses that accompanied splenomegaly lacked a clonal T-cell population, and were found to be predominantly from the B-cell lineage, with Burkitt lymphoma, follicular B-cell lymphoma, and multiple myeloma (i.e., plasma-cell tumors) all identified. Importantly, these B cells did not show Cre-mediated loss of endogenous MYC, and showed high pS62 MYC staining presumably from endogenous MYC, indicating that they were not directly driven by expression of the MYC^{S62A} transgene. No MYC^{WT} and only one $MYC^{WT}MYC^{fl/fl}$ mouse developed a thymic lymphoma in our model indicating that normal regulation of the ectopically expressed MYC^{WT} protein is nontumorigenic at levels driven by the ROSA promoter. This underscores the functional relevance of regulated phosphorylation at S62 and T58.

In contrast to $MYC^{S62A}MYC^{fl/fl}$ mice in which loss of endogenous *Myc* resulted in reduced total thymocytes and a lower level of T-cell lymphomagenesis, we saw a more rapid onset of T-cell lymphoma and decreased survival in $MYC^{T58A}MYC^{fl/fl}$ mice lacking endogenous *Myc*. This finding indicates that endogenous *Myc* dampens the tumorigenic effects of MYC^{T58A}, suggesting that the possibility of MYC-MAX heterodimers (53) forming with either endogenous MYC or MYC^{T58A} in the transcriptional machinery suppresses tumor onset in our model. The differential effect of the presence of endogenous *Myc* on lymphomagenesis in MYC^{S62A} versus MYC^{T58A} mice suggests altered transcriptional regulatory activity between these phosphorylation site mutants. This is consistent with the role of S62 phosphorylation in directing MYC promoter binding and activated gene expression (14, 70). In addition, our previous studies indicated that regulated sequential phosphorylation of S62 and T58 is important for both temporal cycling of MYC on and off target genes and the spatial regulation of MYC to associate with a subset of target genes located near the nuclear pore complexes (14, 70). In these studies, the MYC^{T58A} and MYC^{S62A} mutants had different temporal and spatial target gene binding, suggesting that they may differentially regulate gene transcription. Indeed, RNA-seq data revealed distinct pathway enrichment between the T-cell lymphomas from $MYC^{T58A}MYC^{fl/fl}$ and $MYC^{S62A}MYC^{fl/fl}$ mice, with enrichment of KRAS, angiogenesis, and IFNα response pathways in the $MYC^{T58A}MYC^{fl/fl}$ tumors, and G_2–M checkpoint, MYC targets, and mitotic spindle pathways in the $MYC^{S62A}MYC^{fl/fl}$ tumors. Thus, MYC^{S62A} appears to drive T-cell lymphomas in our model through the dysregulation of cell-cycle checkpoint, upregulation of MYC targets, and mitotic spindle genes.

A diverging pattern of gene expression was also seen when comparing thymic masses in $MYC^{S62A}MYC^{fl/fl}$ mice presenting with splenomegaly, showing an enrichment of IFNα and γ gene sets consistent with the etiologic differences between these thymic masses that were predominantly malignant B cells. The mechanism for B-cell lymphomagenesis and infiltration of B cells into the thymic cavity in $MYC^{S62A}MYC^{fl/fl}$ mice still remains to be elucidated. However, based on our observations in early thymic development in $MYC^{S62A}MYC^{fl/fl}$ mice of reduced total thymocytes and *ex vivo* proliferation, we would hypothesize that the expression of MYC^{S62A} contributes to an initial defect in T-cell proliferation that allows for the mis-regulation and expansion of the B-cell population which, in some cases resulted in terminally differentiated plasma B cells. This B-cell lymphomagenesis appears to be independent of leaky transgene expression and is probably due to the interdependencies of T- and B-cell development *in vivo*.

Multiple studies have shown the oncogenic potential of MYC^{T58A} and the importance of S62 phosphorylation in the regulation, transcriptional activity, and degradation of MYC. In this study, we demonstrate for the first time, the ability of the MYC^{S62A} mutant to directly drive T-cell lymphomas in a mouse model. Despite a significantly lower penetrance, a portion of $MYC^{S62A}MYC^{fl/fl}$ mice developed rapid clonal T-cell lymphomas. Conversely, we also observed defects in T-cell proliferation and expansion *ex vivo* and *in vivo* in the $MYC^{S62A}MYC^{fl/fl}$ mice and that this defect in proper T-cell development was indirectly associated with progressive B-cell lymphomas originating from the spleen. These mechanisms remain to be elucidated, however, these results reaffirm the importance of MYC in T- and B-cell biology and human disease, and demonstrate the protumorigenic properties of posttranslationally deregulated MYC (8, 9, 20, 29, 32, 68).

Authors' Disclosures

S.A. Byers reports grants from NIH; and grants from Collins Medical Trust during the conduct of the study. E. Juarez reports grants from NIEHS during the conduct of the study. L.M. Coussens reports personal fees and nonfinancial support from Cell Signaling Technologies; nonfinancial support and other support from ZellBio, Inc., Syndax Pharmaceuticals Inc.; personal fees, nonfinancial support, and other support from Hibercell, Inc.; other support from Prospect Creek Foundation, Lustgarten Foundation for Pancreatic Cancer Research, Pharmacyclics, Inc. (steering committee for PCYC-1137-CA), AstraZeneca Partner of Choice Network, Cancer Research Institute, The V Foundation for Cancer Research, American Association for Cancer Research (AACR), AACR (Cancer Discovery); personal fees and other support from Susan G. Komen Foundation; personal fees from Carisma Therapeutics Inc., Verseau Therapeutics, Inc., CytomX Therapeutics, Inc., Kineta Inc., Alkermes, Inc., PDX Pharmaceuticals, Inc., Zymeworks, Inc., Genenta Sciences, Pio Therapeutics Pty Ltd., (P30) Koch Institute for Integrated Cancer Research, Massachusetts Institute of Technology, Bloomberg-Kimmel Institute for Cancer Immunotherapy, Sidney Kimmel Comprehensive Cancer Center at Johns Hopkins (Baltimore, MD), (P50) Dana-Farber Cancer Center Breast SPORE (Boston, MA), (P30) Dana-Farber/Harvard Cancer Center, (P30) University of California, San Diego Moores Cancer Center (San Diego, CA), (P30) The Jackson Laboratory Cancer Center, (P01) Columbia University Medical Center (New York, NY), (P50) MDACC GI SPORE, Lustgarten Foundation for Pancreatic Cancer Research (Therapeutics Working Group), NIH/NCI-Frederick National Laboratory Advisory Committee, AbbVie Inc., Shasqi, Inc., AACR (Cancer Immunology Research); and other support from Cancer Cell during the conduct of the study. R.C. Sears reports grants from NIH, Leukemia and Lymphoma Society; and grants from Brenden-Colson Center Foundation during the conduct of the study. No disclosures were reported by the other authors.

Authors' Contributions

C.J. Daniel: Conceptualization, data curation, formal analysis, investigation, visualization, methodology, writing–original draft, writing–review and editing. **C. Pelz:** Formal analysis. **X. Wang:** Data curation. **M.W. Munks:** Data curation, writing–review and editing. **A. Ko:** Data curation, writing–review and editing. **D. Murugan:** Data curation. **S.A. Byers:** Conceptualization. **E. Juarez:** Software. **K.L. Taylor:** Project administration, writing–review and editing. **G. Fan:** Formal analysis. **L.M. Coussens:** Resources, funding acquisition. **J.M. Link:** Methodology, writing–review and editing. **R.C. Sears:** Supervision, funding acquisition, investigation, writing–review and editing.

Acknowledgments

We would like to thank Dr. Peter Hurlin for providing the *Myc* null mice and members of the Sears lab for helpful suggestions and edits. These studies were supported by funding from the Leukemia and Lymphoma Society and the NIH/NCI (grant nos. R01 CA129040, R01 CA186241, R01 CA196228, U01 CA224012, and U54 CA209988), and the OHSU–Brenden-Colson Center for Pancreatic Care to R.C. Sears, NIH/NCI (grant nos. U01 CA224012, and U2C CA233280), the Knight Cancer Institute, and the OHSU–Brenden-Colson Center for Pancreatic Care to L.M. Coussens, and the Knight NCI Cancer Center Support Grant 5P30CA069533.

The costs of publication of this article were defrayed in part by the payment of page charges. This article must therefore be hereby marked *advertisement* in accordance with 18 U.S.C. Section 1734 solely to indicate this fact.

Received July 16, 2021; revised March 1, 2022; accepted March 29, 2022; published first April 5, 2022.

References

1. Eilers M, Eisenman RN. Myc's broad reach. Genes Dev 2008;22:2755–66.
2. Arvanitis C, Felsher DW. Conditional transgenic models define how MYC initiates and maintains tumorigenesis. Semin Cancer Biol 2006;16:313–7.
3. Grandori C, Cowley SM, James LP, Eisenman RN. The Myc/Max/Mad network and the transcriptional control of cell behavior. Annu Rev Cell Dev Biol 2000;16:653–99.
4. Nesbit CE, Tersak JM, Prochownik EV. MYC oncogenes and human neoplastic disease. Oncogene 1999;18:3004–16.
5. Chrzan P, Skokowski J, Karmolinski A, Pawelczyk T. Amplification of c-myc gene and overexpression of c-Myc protein in breast cancer and adjacent non-neoplastic tissue. Clin Biochem 2001;34:557–62.
6. Chou TY, Hart GW, Dang CV. c-Myc is glycosylated at threonine 58, a known phosphorylation site and a mutational hot spot in lymphomas. J Biol Chem 1995;270:18961–5.
7. Bahram F, von der Lehr N, Cetinkaya C., Larsson LG. c-Myc hot spot mutations in lymphomas result in inefficient ubiquitination and decreased proteasome-mediated turnover. Blood 2000;95:2104–10.
8. Nguyen L, Papenhausen P, Shao H. The role of c-MYC in B-cell lymphomas: diagnostic and molecular aspects. Genes 2017;8:116.
9. Filip D, Mraz M. The role of MYC in the transformation and aggressiveness of "indolent" B-cell malignancies. Leuk Lymphoma 2020;61:510–24.
10. Sears RC. The life cycle of C-myc: from synthesis to degradation. Cell Cycle Georget Tex 2004;3:1133–7.
11. Farrell AS, Sears RC. MYC degradation. Cold Spring Harb Perspect Med 2014;4:a014365.
12. Sears R, Nuckolls F, Haura E, Taya Y, Tamai K, Nevins JR. Multiple Ras-dependent phosphorylation pathways regulate Myc protein stability. Genes Dev 2000;14:2501–14.
13. Devaiah BN, Mu J, Akman B, Uppal S, Weissman JD, Cheng D, et al. MYC protein stability is negatively regulated by BRD4. Proc Natl Acad Sci U S A 2020;117:13457–67.
14. Farrell AS, Pelz C, Wang X, Daniel CJ, Wang Z, Su Y, et al. Pin1 regulates the dynamics of c-Myc DNA binding to facilitate target gene regulation and oncogenesis. Mol Cell Biol 2013;33:2930–49.
15. Arnold HK, Zhang X, Daniel CJ, Tibbitts D, Escamilla-Powers J, Farrell A, et al. The Axin1 scaffold protein promotes formation of a degradation complex for c-Myc. EMBO J 2009;28:500–12.
16. Zhang X, Farrell AS, Daniel CJ, Arnold H, Scanlan C, Laraway BJ, et al. Mechanistic insight into Myc stabilization in breast cancer involving aberrant Axin1 expression. Proc Natl Acad Sci U S A 2012;109:2790–5.
17. Hart MJ, de los Santos R, Albert IN, Rubinfeld B, Polakis P. Downregulation of beta-catenin by human Axin and its association with the APC tumor suppressor, beta-catenin and GSK3 beta. Curr Biol CB 1998;8:573–81.
18. Nakamura T, Hamada F, Ishidate T, Anai K, Kawahara K, Toyoshima K, et al. Axin, an inhibitor of the Wnt signalling pathway, interacts with beta-catenin, GSK-3beta and APC and reduces the beta-catenin level. Genes Cells 1998;3:395–403.
19. O'Neil J, Grim J, Strack P, Rao S, Tibbitts D, Winter C, et al. FBW7 mutations in leukemic cells mediate NOTCH pathway activation and resistance to gamma-secretase inhibitors. J Exp Med 2007;204:1813–24.
20. Malempati S, Tibbitts D, Cunningham M, Akkari Y, Olson S, Fan G, et al. Aberrant stabilization of c-Myc protein in some lymphoblastic leukemias. Leukemia 2006;20:1572–81.
21. Agarwal A, MacKenzie RJ, Pippa R, Eide CA, Oddo J, Tyner JW, et al. Antagonism of SET using OP449 enhances the efficacy of tyrosine kinase inhibitors and overcomes drug resistance in myeloid leukemia. Clin Cancer Res 2014;20:2092–103.
22. Arnold HK, Sears RC. A tumor suppressor role for PP2A-B56alpha through negative regulation of c-Myc and other key oncoproteins. Cancer Metastasis Rev 2008;27:147–58.
23. Arnold HK, Sears RC. Protein phosphatase 2A regulatory subunit B56alpha associates with c-myc and negatively regulates c-myc accumulation. Mol Cell Biol 2006;26:2832–44.
24. Chang DW, Claassen GF, Hann SR, Cole MD. The c-Myc transactivation domain is a direct modulator of apoptotic versus proliferative signals. Mol Cell Biol 2000;20:4309–19.
25. Pulverer BJ, Fisher C, Vousden K, Littlewood T, Evan G, Woodgett JR. Site-specific modulation of c-Myc cotransformation by residues phosphorylated in vivo. Oncogene 1994;9:59–70.
26. Thibodeaux CA, Liu X, Disbrow GL, Zhang Y, Rone JD, Haddad BR, et al. Immortalization and transformation of human mammary epithelial cells by a tumor-derived Myc mutant. Breast Cancer Res Treat 2009;116:281–94.
27. Yeh E, Cunningham M, Arnold H, Chasse D, Monteith T, Ivaldi G, et al. A signalling pathway controlling c-Myc degradation that impacts oncogenic transformation of human cells. Nat Cell Biol 2004;6:308–18.

28. Wasylishen AR, Stojanova A, Oliveri S, Rust AC, Schimmer AD, Penn LZ. New model systems provide insights into Myc-induced transformation. Oncogene 2011;30:3727–34.
29. Wang X, Cunningham M, Zhang X, Tokarz S, Laraway B, Troxell M, et al. Phosphorylation regulates c-Myc's oncogenic activity in the mammary gland. Cancer Res 2011;71:925–36.
30. Link JM, Ota S, Zhou Z-Q, Daniel CJ, Sears RC, Hurlin PJ. A critical role for Mnt in Myc-driven T-cell proliferation and oncogenesis. Proc Natl Acad Sci U S A 2012;109:19685–90.
31. Chakraborty AA, Scuoppo C, Dey S, Thomas LR, Lorey SL, Lowe SW, et al. A common functional consequence of tumor-derived mutations within c-MYC. Oncogene 2015;34:2406–9.
32. La Starza R, Borga C, Barba G, Pierini V, Schwab C, Matteucci C, et al. Genetic profile of T-cell acute lymphoblastic leukemias with MYC translocations. Blood 2014;124:3577–82.
33. Weng AP, Ferrando AA, Lee W, Morris JP, Silverman LB, Sanchez-Irizarry C, et al. Activating mutations of NOTCH1 in human T cell acute lymphoblastic leukemia. Science 2004;306:269–71.
34. Herranz D, Ambesi-Impiombato A, Palomero T, Schnell SA, Belver L, Wendorff AA, et al. A NOTCH1-driven MYC enhancer promotes T cell development, transformation and acute lymphoblastic leukemia. Nat Med 2014;20:1130–7.
35. Jones RG, Thompson CB. Revving the engine: signal transduction fuels T cell activation. Immunity 2007;27:173–8.
36. Li Q, Pan S, Xie T, Liu H. MYC in T-cell acute lymphoblastic leukemia: functional implications and targeted strategies. Blood Sci 2021;3:65–70.
37. MacDonald HR, Wilson A, Radtke F. Notch1 and T-cell development: insights from conditional knockout mice. Trends Immunol 2001;22:155–60.
38. Sanchez-Martin M, Ferrando A. The NOTCH1-MYC highway toward T-cell acute lymphoblastic leukemia. Blood 2017;129:1124–33.
39. Ashton GH, Morton JP, Myant K, Phesse TJ, Ridgway RA, Marsh V, et al. Focal adhesion kinase is required for intestinal regeneration and tumorigenesis downstream of Wnt/c-Myc signaling. Dev Cell 2010;19:259–69.
40. Myant K, Qiao X, Halonen T, Come C, Laine A, Janghorban M, et al. Serine 62-phosphorylated MYC associates with nuclear lamins and its regulation by CIP2A Is essential for regenerative proliferation. Cell Rep 2015;12:1019–31.
41. Shimizu C, Kawamoto H, Yamashita M, Kimura M, Kondou E, Kaneko Y, et al. Progression of T cell lineage restriction in the earliest subpopulation of murine adult thymus visualized by the expression of lck proximal promoter activity. Int Immunol 2001;13:105–17.
42. de Alboran IM, O'Hagan RC, Gärtner F, Malynn B, Davidson L, Rickert R, et al. Analysis of C-MYC function in normal cells via conditional gene-targeted mutation. Immunity 2001;14:45–55.
43. Dose M, Khan I, Guo Z, Kovalovsky D, Krueger A, von Boehmer H, et al. c-Myc mediates pre-TCR-induced proliferation but not developmental progression. Blood 2006;108:2669–77.
44. Daniel CJ, Sun XX, Chen Y, Zhang X, Dai MS, Sears RC. Detection of post-translational modifications on MYC. Methods Mol Biol 2021;2318:69–85.
45. Jinadasa R, Balmus G, Gerwitz L, Roden J, Weiss R, Duhamel G. Derivation of thymic lymphoma T-cell lines from Atm(-/-) and p53(-/-) mice. J Vis Exp JoVE 2011;50:2598.
46. Daniel CJ, Zhang X, Sears RC. Detection of c-Myc protein-protein interactions and phosphorylation status by immunoprecipitation. Methods Mol Biol 2013;1012:65–76.
47. Medler TR, Murugan D, Horton W, Kumar S, Cotechini T, Forsyth AM, et al. Complement C5a fosters squamous carcinogenesis and limits T cell response to chemotherapy. Cancer Cell 2018;34:561–78.
48. Subramanian A, Tamayo P, Mootha VK, Mukherjee S, Ebert BL, Gillette MA, et al. Gene set enrichment analysis: a knowledge-based approach for interpreting genome-wide expression profiles. Proc Natl Acad Sci U S A 2005;102:15545–50.
49. Liberzon A, Subramanian A, Pinchback R, Thorvaldsdóttir H, Tamayo P, Mesirov JP. Molecular signatures database (MSigDB) 3.0. Bioinforma 2011;27:1739–40.
50. Godec J, Tan Y, Liberzon A, Tamayo P, Bhattacharya S, Butte AJ, et al. Compendium of immune signatures identifies conserved and species-specific biology in response to inflammation. Immunity 2016;44:194–206.
51. Wang X, Langer EM, Daniel CJ, Janghorban M, Wu V, Wang XJ, et al. Altering MYC phosphorylation in the epidermis increases the stem cell population and contributes to the development, progression, and metastasis of squamous cell carcinoma. Oncogenesis 2020;9:79.
52. Kortlever RM, Sodir NM, Wilson CH, Burkhart DL, Pellegrinet L, Swigart LB, et al. Myc cooperates with Ras by programming inflammation and immune suppression. Cell 2017;171:1301–15.
53. Nair SK, Burley SK. Structural aspects of interactions within the Myc/Max/Mad network. Curr Top Microbiol Immunol 2006;302:123–43.
54. Carow B, Gao Y, Coquet J, Reilly M, Rottenberg ME. lck-driven Cre expression alters T cell development in the thymus and the frequencies and functions of peripheral T cell subsets. J Immunol 2016;197:2261–8.
55. Dang CV. MYC, metabolism, cell growth, and tumorigenesis. Cold Spring Harb Perspect Med 2013;3:a014217;3:a014217.
56. Rudolph B, Hueber AO, Evan GI. Reversible activation of c-Myc in thymocytes enhances positive selection and induces proliferation and apoptosis in vitro. Oncogene 2000;19:1891–900.
57. Michalek RD, Rathmell JC. The metabolic life and times of a T-cell. Immunol Rev 2010;236:190–202.
58. Yu Q, Erman B, Park JH, Feigenbaum L, Singer A. IL-7 receptor signals inhibit expression of transcription factors TCF-1, LEF-1, and RORgammat: impact on thymocyte development. J Exp Med 2004;200:797–803.
59. Wilmore JR, Jones DD, Allman D. Protocol for improved resolution of plasma cell subpopulations by flow cytometry. Eur J Immunol 2017;47:1386–8.
60. Pracht K, Meinzinger J, Daum P, Schulz SR, Reimer D, Hauke M, et al. A new staining protocol for detection of murine antibody-secreting plasma cell subsets by flow cytometry. Eur J Immunol 2017;47:1389–92.
61. Sharma S, Zhu J. Immunologic applications of conditional gene modification technology in the mouse. Curr Protoc Immunol 2014;105:10.34.1–10.34.13.
62. Douglas NC, Jacobs H, Bothwell AL, Hayday AC. Defining the specific physiological requirements for c-Myc in T cell development. Nat Immunol 2001;2:307–15.
63. Malynn BA, de Alboran IM, O'Hagan RC, Bronson R, Davidson L, DePinho RA, et al. N-myc can functionally replace c-myc in murine development, cellular growth, and differentiation. Genes Dev 2000;14:1390–9.
64. Sheppard RD, Samant SA, Rosenberg M, Silver LM, Cole MD. Transgenic N-myc mouse model for indolent B cell lymphoma: tumor characterization and analysis of genetic alterations in spontaneous and retrovirally accelerated tumors. Oncogene 1998;17:2073–85.
65. Del Prete G, Telford JL, Baldari CT, Majolini MB, D'Elios MM, Galieni P, et al. Specific tyrosine kinase Lck in normal B-1 cells- expression of the T-cell. Blood 1998;91:3390–6.
66. Majolini MB, D'Elios MM, Galieni P, Boncristiano M, Lauria F, Del Prete G, et al. Expression of the T-cell-specific tyrosine kinase Lck in normal B-1 cells and in chronic lymphocytic leukemia B cells. Blood 1998;91:3390–6.
67. Ulivieri C, Valensin S, Majolini MB, Matthews RJ, Baldari CT. Normal B-1 cell development but defective BCR signaling in Lck-/- mice. Eur J Immunol 2003;33:441–5.
68. Kalkat M, De Melo J, Hickman KA, Lourenco C, Redel C, Resetca D, et al. MYC deregulation in primary human cancers. Genes 2017;8:151.
69. Masuda K, Kakugawa K, Nakayama T, Minato N, Katsura Y, Kawamoto H. T cell lineage determination precedes the initiation of TCRβ gene rearrangement. J Immunol 2007;179:3699–706.
70. Su Y, Pelz C, Huang T, Torkenczy K, Wang X, Cherry A, et al. Post-translational modification localizes MYC to the nuclear pore basket to regulate a subset of target genes involved in cellular responses to environmental signals. Genes Dev 2018;32:1398–419.